A high current cathode plasma jet flow model for the Pulsed Plasma Thruster

IEPC-2011-114

Presented at the 32nd International Electric Propulsion Conference,
Wiesbaden, Germany
September 11–15, 2011

Shaw P. V. [*] and Lappas V. J. [†]
University of Surrey, Guildford, Surrey, GU2 7XH, UK

Experimental studies with a Pulsed Plasma Thruster have shown that the ratio between the electromagnetic contribution of the impulse bit between a parallel plate breech fed PPT with Teflon^{TM} to without Teflon^{TM} is around 0.60 to 0.75 over the experimental range conducted. Without Teflon^{TM} the plasma for the PPT discharge originates from the erosion of the electrodes. To model a PPT without the presence of Teflon^{TM} a lumped circuit analysis model approach was used to describe the individual elements of the PPT. Once broken down a series of sub-models were applied to each element to describe their electrical or physical properties. Sub-models included; an empirical estimation for the capacitor as a function of discharge frequency, an impedance model for the electrodes calculating their resistance, self inductance and mutual inductance with each other, a Lorentz force model based on a non uniform magnetic field, an electrode mass erosion model based on cathode spot erosion, an electrode sheath model to describe the charge limitation effects of the plasma sheath and finally a simplified hydrodynamic model applied to a plasma flow model that took account of pinching effects from the high current plasma. The model was validated against experimental results to show its validity for predicting the performance of a PPT discharge. Finally the model was used to probe the internal dynamics and processes that may occur within the PPT discharge.

[*]Research Assistant, Surrey Space Centre, p.shaw@surrey.ac.uk
[†]Reader, Surrey Space Centre, v.lappas@surrey.ac.uk

Nomenclature

k_B = Boltzmann constant, JK^{-1}
e = Elimentary charge, C
e_0 = Vacuum permittivity of free space, Fm^{-1}
g_0 = Gravitational constant, ms^{-2}
μ_{Earth} = Standard gravitational parameter, m^3s^{-2}
μ_0 = Magnetic permeability of free space, NA^{-2}
α_i = Ion current normalised by arc current, %
ϵ = Electromotive force, V
ϵ = Permittivity, Fm^-1
ρ = Mass density, kgm^{-3}
ϕ_B = Magnetic flux, Vs
Φ_{wall} = Potential of the wall, V
Ω = Magnetic gyration frequency, Hz
ω_p = Plasma frequency of particle species, Hz
ω_{pulse} = Frequency of pulse discharge, Hz
σ_{sub} = Sub conductor conductivity, $\Omega^{-1}m^{-1}$
σ = Electrical conductivity, $\Omega^{-1}m^{-1}$
τ = Characteristic time of the pulse discharge, s
τ_L = Characteristic ion particle time of flight across inter-electrode gap, s
τ_S = Characteristic time of relaxation of ion charge states from cathode spot to quasi steady state value, s
υ_{ie} = Electron ion collision frequency, Hz
Γ_i = Ion erosion rate, kgC^{-1}
A = Area of the conductor plate, m^2
B = Magnetic field, T
C = Capacitance of the PPT capacitor, F
C_n = Accumulated ion fraction distribution at freezing zone of the $\sum n^{th}$ levels
D_0 = Electric displacement field, Cm^{-2}
D_0 = Electric field strength, Vm^{-1}
d = Distance between the capacitor conductors/plates, m
d_{sheath} = Sheath thickness, m
E = Energy of the PPT discharge, J
F_{PPT} = Force produced by the PPT, N
f_n = Charge state fraction along the axis from the cathode of the n^{th} level
f_n^0 = Charge state fraction distribution at the freezing zone of the n^{th} level
h = Separation distance between electrodes, m
I = Circuit loop current, A
I_{arc} = Arc current flowing through the circuit loop, A
I_{bit} = Impulse generated per discharge, Ns
$I_{i,n}$ = Ionisation energy to take an ion from the $n-1$ state to the n charge state
I_{sp} = Specific impulse, s
I_{spot} = Current associated with each cathode spot, A
J = Current density, Am^{-2}
k_n = Ionisation coefficient of the n^{th} charge state level
L = Impulse, Ns
$L_{circuit}$ = Inductance of the circuit, H
L' = Inductance per unit length, Hm^{-1}

M = Mach number
M_{bit} = Mass eroded per discharge, kg
$M_{Propellant}$ = Propellant mass, kg
M_{Sat} = Satellite mass, kg
m = Total mass contained within the 'plasma flow', kg
m_j = Particle mass of species j, kg
m_e = Electron mass, kg
N_e = Electron density, m^{-3}
N_j = Electron density of particle species j, m^{-3}
N_{Pulses} = Total pulse number provided by the PPT
P = Plasma pressure, Nm^{-2}
Q = Charge on the Capacitor conductors/plates, C
Q_{ei} = Electron energy losses under elastic and inelastic electron-ion collisions, J
$\overline{Q_0}$ = Initial ion charge state number in plasma jet
$\overline{Q}$ = Mean ion charge state number in plasma flow
Q_n = Ion charge state at the n^{th} ionisation level
R = Radius of the plasma flow where the plasma pressure equals the constraining magnetic pressure, m
$R_{circuit}$ = Resistance of the circuit, Ω
S_0 = Surface area of the initial plasma flow near the mixing region, m^2
S_{spot} = Surface area of the cathode spot near the mixing region, m^2
T_{cr} = Critical electron temperature in the plasma flow, K
T_e = Electron temperature, K
T_m = Maximum electron temperature in the plasma jet, K
t = Time, s
u_e = Exhaust speed, ms^{-1}
V = Bulk plasma velocity, ms^{-1}
V = Voltage applied across the Capacitor, V
V_e = Electron velocity, ms^{-1}
w = Electrode width, m
z = Distance from the cathode along the axis that joins the cathode to the anode, m
z_0 = Distance above cathode that the plasma mixing region is located, m

I. Introduction

Parallel to the developmental and experimental work conducted as the Surrey Space Centre,[1,2] modelling of a PPT discharge has also been an ongoing project. Modelling within the PPT field has been diverse. Developed models include the analysis of the interaction between the Teflon^{TM} surface and the plasma bulk via a layer model,[3,4] the expansion and evolution of the plasma plume,[5,6] return of carbon molecules to the Teflon^{TM} surface,[7] complete three dimensional MHD modelling of the PPT discharge[8,9] and numerous one dimensional models based on the snowplow and mass slug-shot models.[10,11] Due to avaliable resources modelling focuused on designing a one dimensional lumped circuit analysis model with a simplified magnetohydrodynamic flow model.

The lumped circuit analysis model is based on separating the PPT thruster into its constituent electrical components and allocating discrete values to these, i.e. the electrode inductance, the mutual electrode inductance, the capacitor inductance etc. Figure 1 shows the mechanical parts of a PPT overlaid with their allocated electrical parameters.

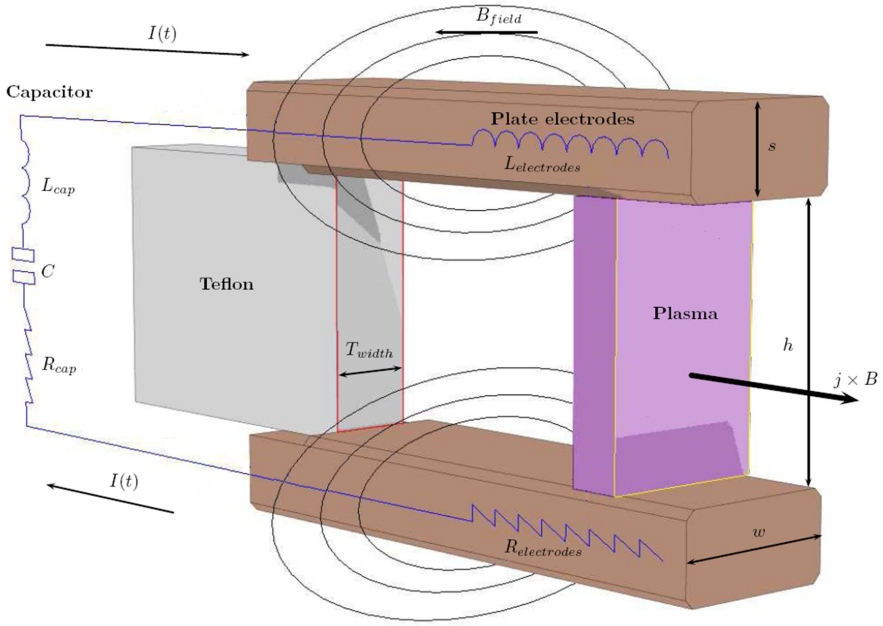

Figure 1. A one dimensional circuit schematic overlaid on the components of a PPT

The one dimensional model is then linked with Newtonian mechanics and a mass model to describe how the plasma mass accelerates out of the discharge chamber. Within this paper each parameter is discussed in detail to understand its origin, its significance and how it interacts with other variables during the discharge process. Once the model is formulated and after it has been validated against the experimental results, the model is used to draw conclusions on processes that are occurring within the PPT discharge. Finally the model is then used to identify trends that can lead to optimise a miniaturised PPT.

II. PPT Model

A. Lumped Circuit Model

Formation of the code begins from first principles. Using the circuit depicted in Figure 1 Faraday's law is applied around the circuit and the direction of the electromotive force, ϵ, is given by Lenz's law:

$$
\begin{aligned}
|\epsilon| &= \left| \frac{d\phi_B}{dt} \right| \\
\epsilon &= -\frac{d}{dt}\left[\phi_B\right] \\
\epsilon &= -\frac{d}{dt}\left[L_{circuit} I\right] \\
\epsilon &= -\left[L_{circuit}\frac{dI}{dt} + I\frac{dL_{circuit}}{dt} \right]
\end{aligned}
\tag{1}
$$

The electromotive force causes the flow of current through the current loop and can be alternatively expressed by the difference between the potential before work has been done by the electromotive force and the potential after work has been done by the electromotive force. Also, by considering Kirchhoff's law, Equation 1 becomes:

$$
\begin{aligned}
V_{after} - V_{before} &= -\left[L_{circuit}\frac{dI}{dt} + I\frac{dL_{circuit}}{dt} \right] \\
V_{before} &= IR_{circuit} + L_{circuit}\frac{dI}{dt} + I\frac{dL_{circuit}}{dt} \\
V_0 - \frac{1}{C_{PPT}}\int (I)dt &= IR_{circuit} + L_{circuit}\frac{dI}{dt} + I\frac{dL_{circuit}}{dt}
\end{aligned}
\tag{2}
$$

The voltage before work is done by the electromotive force can be realised as being the voltage at time t within the circuit loop. The circuit inductance and resistance can be expressed respectively as:

$$
L_{circuit} = L_{capacitor} + L_{electrodes} + L_{plasma} \tag{3}
$$

$$
R_{circuit} = R_{capacitor} + R_{electrodes} + R_{plasma} \tag{4}
$$

The inductance of the plasma, L_{plasma}, is found from the magnetic flux through the plasma. However, for a closed surface (i.e. a Gaussian surface surrounding the plasma bulk), the magnetic flux is zero:

$$
L_{plasma} = \frac{\phi_B}{I} = \frac{1}{I}\oint B.dS = 0 \tag{5}
$$

B. Capacitor Model

One area of this work, which has not been explored in detail, is the modelling of the contribution that the capacitor makes to the total circuit inductance and resistance. These values are highly dependant on the manufacturing process, the internal electrode geometry, the method of external connection to the rest of the circuit and the dielectric of the capacitor. After initial investigations looking at using a SPICE model to reflect the higher order frequency behaviour mechanisms of a capacitor, it was concluded that this diversion from the focus of the work would be too costly in resources. The SPICE model for each capacitor would need to be custom built and the publically available information required for each component of the capacitor SPICE model is limited. A generic model would be difficult to create and so was left for future work.

As the resistance and inductance contributions from the capacitor were significant, these were measured experimentally using a HM8018 HAMEG Instruments LCR meter. Figure 2 shows a log plot of the capacitor resistance and a log plot of the capacitor inductance as a function of driving frequency. By fitting the data to a polynomial best fit and extrapolating at the discharge frequency ot the PPT (136kHz), an estimation of 33mΩ for the capacitor resistance and 310nH for the capacitor inductance was made.

C. Electrode Model

Modelling the electrode inductance and resistance was not a straight forward procedure. The discharge occurs in the kilohertz regime and at these frequencies the skin depth is small. At 100kHz the skin depth is around 0.2mm for copper. The skin depth is the distance from the surface in which most of the current flows and is due to the skin effect. The skin effect is caused by rotating eddy currents that are formed by

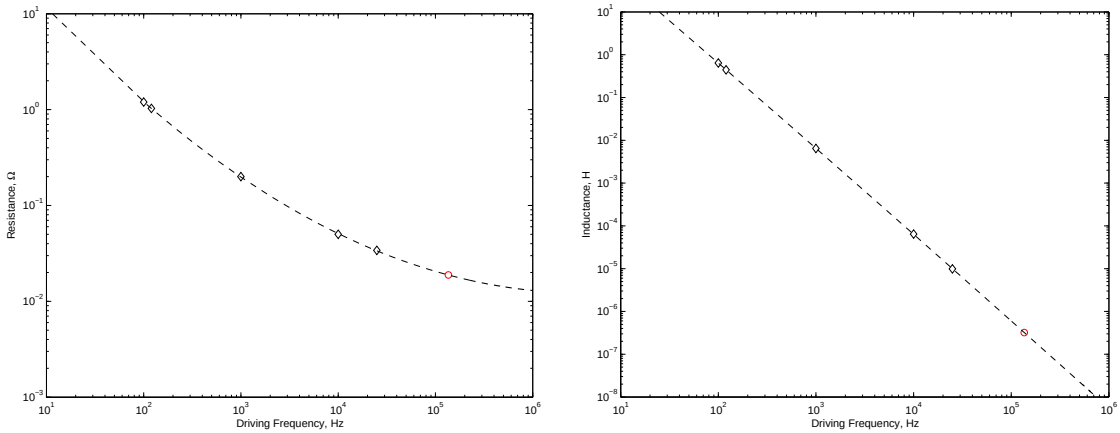

Figure 2. Measured as a function of driving frequency. Left: Capacitor resistance, Right: Capacitor inductance. The black diamonds represent the experimental data from the LCR meter and the red circle represents the extrapolated parameter at 136kHz

free electrons rotating around field lines setup by a fluctuating H-field within the conductor. The pushing of the current to the outer edges of the conductor causes the impedance and inductance of the electrode to be frequency dependant. The model that is used in this work is based on research within the microchip industry which model the high frequency effects between rectangular contacts.[12] The electrodes are split into an array of sub conductors, see Figure 3. The different colours give a visual representation of how the current is distributed in a rectangular high frequency driven conducting post (electrode). Assuming the dimensions chosen for the sub conductor width and length are sufficiently small, with respect to the skin depth at a particular driving frequency, it can be assumed that the current through each sub conductor is constant.

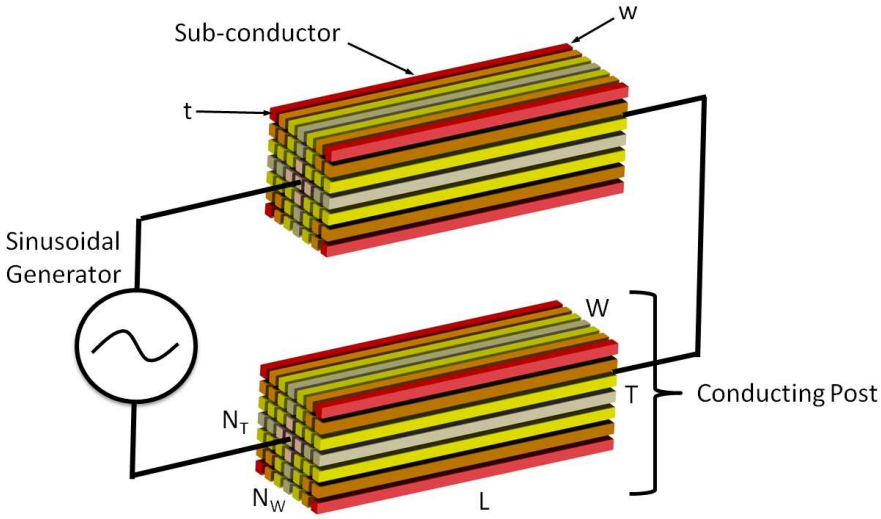

Figure 3. Two conducting posts in series driven by a sinosodial generator

During initial testing of the electrode inductance model it was shown that as the frequency (i.e. the value of the complex component of the inductances) was increased, the model became unstable if the total number of sub conductors was too low. The solution was to increase the number of sub conductors but with this came an increase in the total compiling time. Figure 4 shows the results using MATLAB of a 968 sub conductor system that took 26 minutes to compile. Due to MATLAB being a 'single' string program the compiling time was defined by the processor of the desktop computer used to run the program.

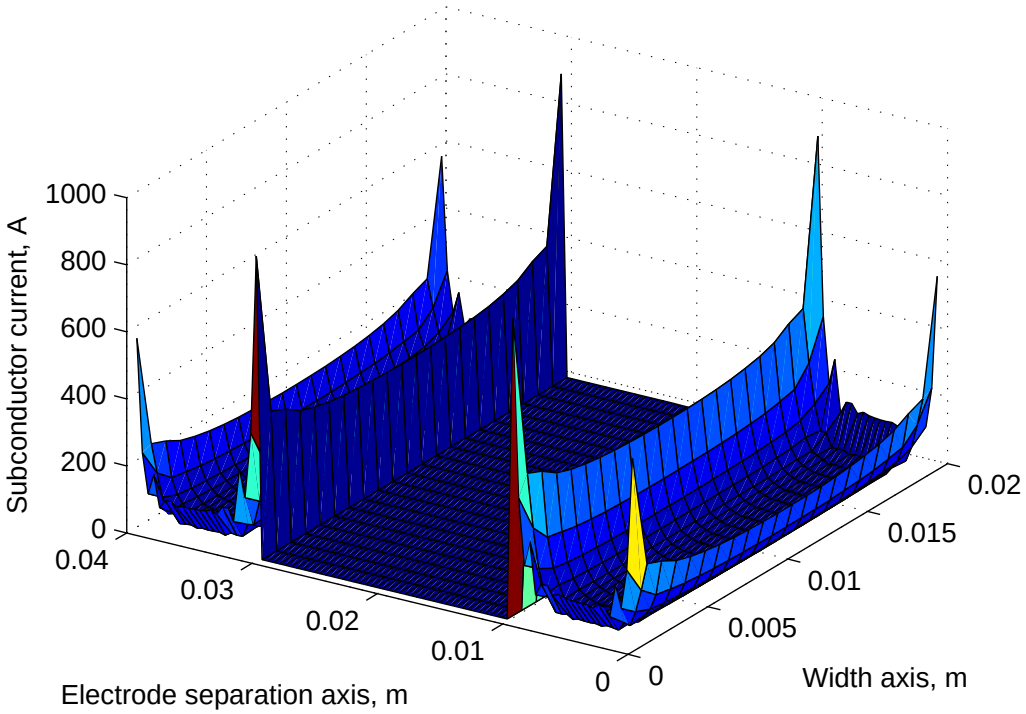

Figure 4. Inductance model based on a PPT discharging at a frequency of 136kHz

Figure 4 clearly shows several features. At 136kHz the current flowing through the centre of the electrodes is minimal. The current tends to flow in the outer regions of the electrode, specifically congregating in the electrode corners. Also due to mutual inductance from the other electrode, an increased proportion of the current flows in the electrode edges located closest to each other than in the outer edges of the electrode. These results coincide with photos of the electrode surface that show increased activity at the electrode edges (i.e. charred edges), see Figure 5.

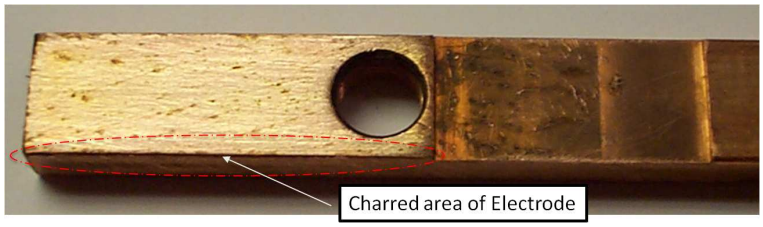

Figure 5. Increased activity on electrode coinciding in the area where high currents are present within the electrode

This model is required to run at every time-step because the inductance model requires voltage and effective electrode length inputs that vary with the discharging capacitor and evolving plasma respectively. It was noted, during model testing, that although the voltage affected the magnitude of the current in each sub conductor, it did not vary the relative sub conductor current magnitudes that the sub conductors shared with each other. It was also observed that the magnitude of the voltage did not affect the inductance or the resistance of the electrode (at 136kHz). This meant that the problem could be reduced to a single variable, the effective electrode length. As the plasma is moved within the discharge chamber it expands the effective length of the current loop. The length between the plasma mass and the capacitor is the effective electrode length and is the part of the electrode that carries current in the current loop. The inductance model was run at several lengths and the electrode resistance and inductance was measured. The points were then fitted to

a curve, see Figure 6. This best fit was used to calculate the inductance and resistance as a function of the effective electrode length based on the PPT which was used in the experiments. Each new PPT electrode geometry would require this process to be undertaken.

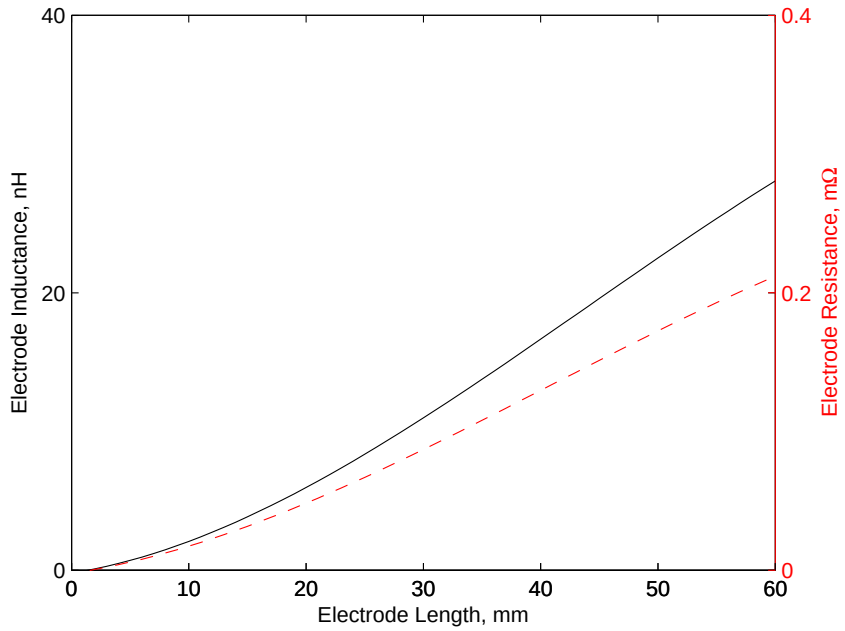

Figure 6. Electrode inductance and resistance as a function of length

It can be seen that the contribution to the total circuit resistance and inductance from the electrodes compared to the experimentally measured capacitor resistance and inductance is minimal. However, the electrode model will be of use when low inductance capacitors are studied and the capacitor and electrode inductances are comparable to each other.

D. Plasma Flow Model

The plasma model was based on observations found in literature and observations made at SSC. The plasma model developed is based on discharges that do not include material between the electrodes (i.e. Teflon^{TM}). In this model it is theorised that the source of the plasma mass originates from the electrode surfaces. High speed photography,[13] electron microscope imagery of electrode craters[1] and photography of electrodes post experimentation (Figure 5) suggest that the electrodes are being eroded in condensed areas by a high energy process, which has a byproduct of crater formation. The high speed photographic images show in detail two structures: first, bright spots that occur on the electrode surface and second, from these bright spots it appears that small but intense jets are formed (seen most clearly on the top electrode at 4800ns and 5100ns, Figure 16).[13]

The model developed to explain these structures draws together experimental and modelling work from two areas based on cathode spot emission sites[14,15] and plasma flows eminating from grouped cathode spot emissions.[16–18] The process starts with the creation of emission centres, i.e. the bright spots seen located on the cathode. The metal electrodes of the PPT are not smooth surfaces on the microscopic scale. Field emission occurs at geometric sharp points and promotes ion bombardment in these locations, see Figure 7. As ion bombardment increases, the emission site rapidly heats and thermionic emissions of electrons occur. The increased presence of electrons promotes further ion bombardment and a thermal runaway occurs. This process rapidly heats the surface of the electrode until it 'explodes' and leaves a visible crater. The crater edge with its rough surface then forms a location for secondary cathode spots to form.

The plasma produced from these 'exploding' bright spots is energetic with the mean ion charge state in the 1+ to 4+ state dependant on the material of the electrode. As the plasma is accelerated and moves away from the emission centre and crater, the plasma transitions from a place of thermal equilibrium to a place

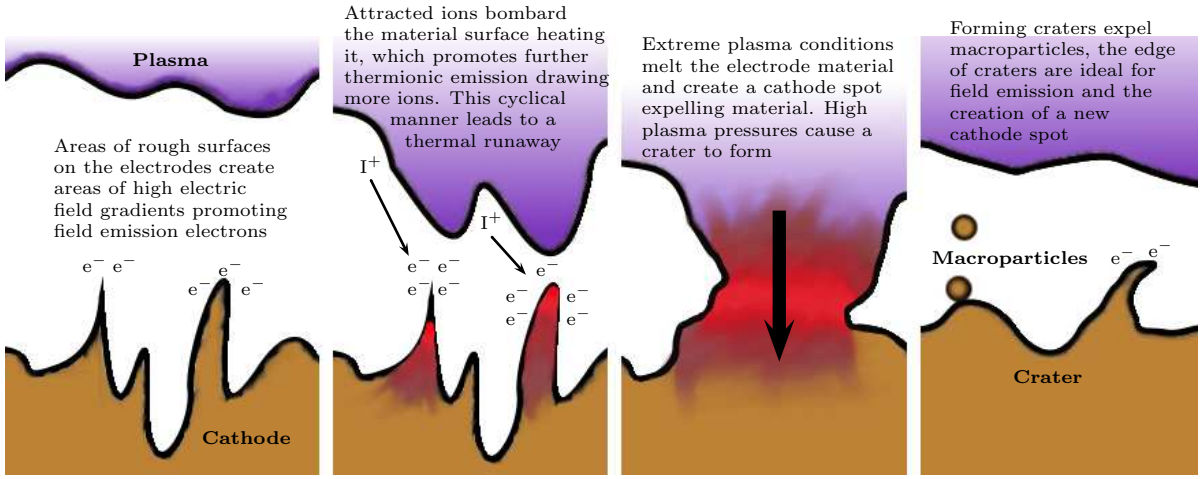

Figure 7. Evolution of the cathode spot process and macro particle formation as a result of plasma pressure on the liquid cathode material

of non-thermal equilibrium. The plasma is assumed to rapidly 'freeze', which means that the parameters of the plasma far from the crater are similar to those close to the crater. The frozen plasma parameters are unique to each element and are summarised by Anders in a periodic table format.[14] The parameters of the frozen plasma for copper are used to describe the plasma conditions close to the cathode electrode in an area known as the mixing region.

The current flowing through the plasma during the discharge, are in the kilo ampere range, which induces a self constricting magnetic field within the plasma flow, see Figure 8. The magnetic force is balanced out by the ideal gas pressure exerted by the highly energetic electrons (known as the Bennet criterion[19]) and a plasma column is created. If the currents are considerable ($\geq$1kA), a sausage instability occurs within the plasma and a pinch forms within the column. The pinch constriction causes a localised area that has an increased particle number density with an increased chance of particle collisions. The increased collision rate causes the particle temperature to rise substantially and further ionise the plasma into higher ion charge states. This is supported by evidence which used an RFEA probe in PPT experiments, where ions up to 199eV were measured in a typical discharge.[20]

The initial plasma parameters originating from the cathode spots using copper electrodes in a PPT are given in Table 1. The initial copper plasma has a velocity of 13.2kms^{-1} towards the direction of the anode and has an average mean ion state of Cu^{2+} (72.1% of the total population).

Table 1. Initial plasma conditions for copper electrodes[21142218]

Initial condition	Value
Cathode Parameters	
Spot splitting current	150±70 A
Plasma Jet	
Mean ion charge state	2.06
Plasma jet radius	1-2 mm
Freezing zone/mixing region	
- Spot velocity	13.2kms^{-1}
- Ion fraction dist.	1+ =10.7%
	2+ =72.1%
	3+ =17.1%
	4+ =0.014%

The number of cathode spots observed during a discharge is proportional to the overall arc current

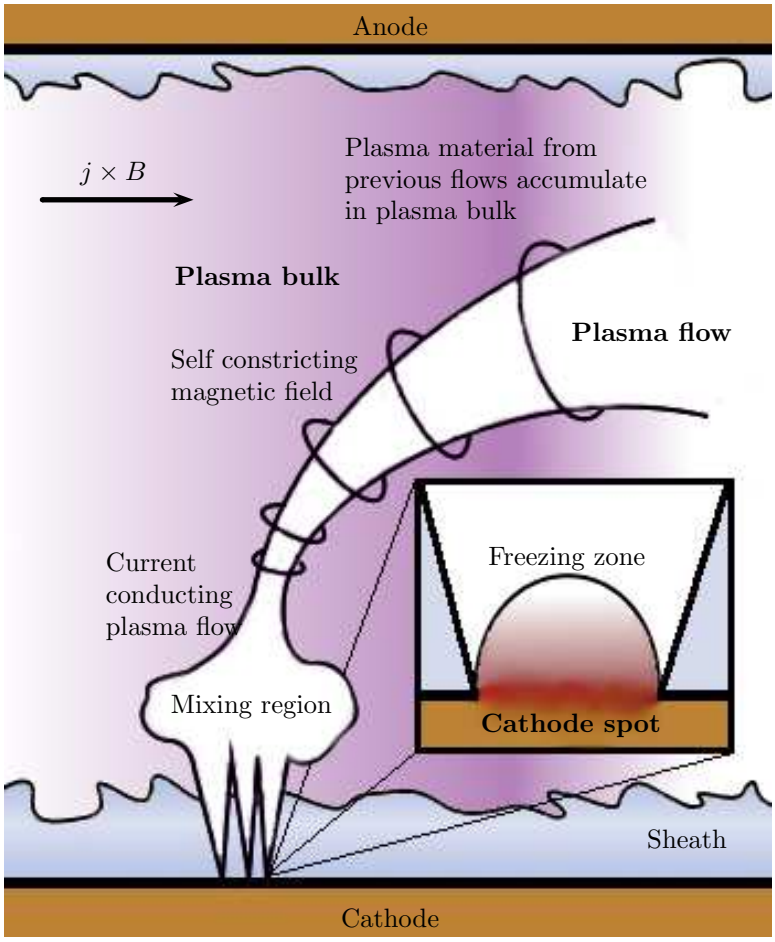

Figure 8. Plasma evolution from emission centre to plasma bulk in a cathode spot plasma flow of a PPT

flowing through the system. For copper electrodes it has been experimentally observed that the current per observed spot, I_{spot}, is 150±70A.[23] If moderate to high currents are flowing through the system a plasma column forms. The column origin, which is in close proximity to the cathode, is an area of increased cathode spot activity. The close proximity of the cathode spots to each other causes their resulting plasma jets to amalgamate into a single 'plasma flow' in an area known as the 'mixing region', located approximately 0.1 to 1mm above the cathode surface.[17]

The 'plasma flow' has dimensions which are dependent on the number of plasma jets present within the discharge (equivalent to the number of cathode spots present). There is limited literature on the dimensions of the micro plasma jets, which originate from the cathode spots and this is the biggest uncertainty introduced into the model presented. The plasma jet is thought to expand parabolically with a circular aperture at its end face. The total area of the flow in the mixing region is taken to be a function of the initial surface area from a single plasma jet (originating from a single cathode spot) multiplied by the total number of cathode spots present in the discharge;

$$S_0 = S_{spot} \frac{I_{arc}}{I_{spot}} \tag{6}$$

An estimate for the dimensions of the individual cathode spot has been found by using a three frame interforic system[22].[21] The radius of the spot can be estimated from the electron density distribution plotted on a equidensitogram, see Figure 9. It shows that the radius of the cathode spot is around 1-2mm for copper.

The plasma flow from the cathode mixing region to the anode sheath is described using a simplified set of magnetohydrodynamic equations. The full set of magnetohydrodynamic equations in three spatial dimensions and one temporal dimension becomes a non trivial task to solve. Simplifications can be made if

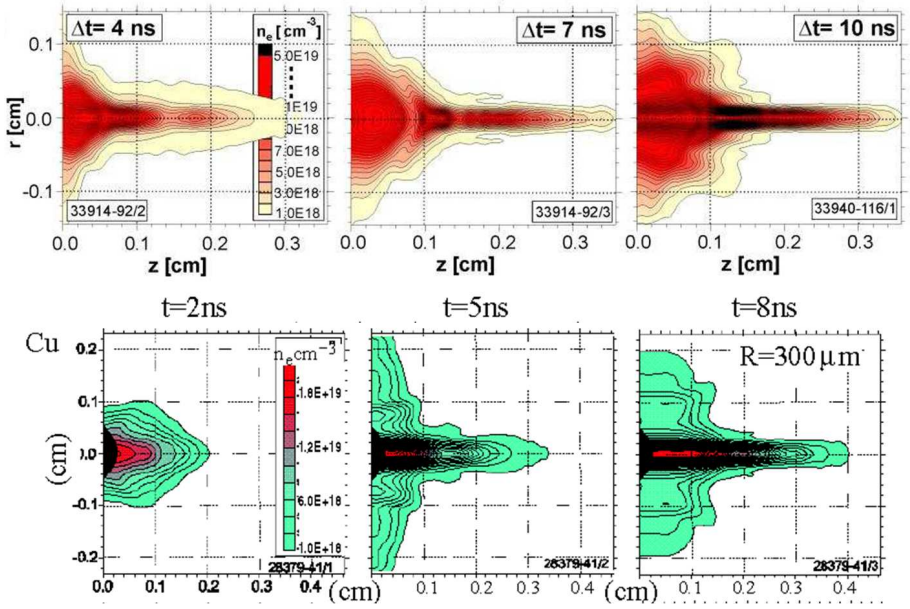

Figure 9. Equidensitograms for copper cathode spots[2221]

it is assumed that the plasma between the electrodes is in a steady state and that the plasma parameters only change with distance from the cathode. The validity of these assumptions needs closer consideration.

The velocity of the ions emitted from the cathode spot region is similar to the ion velocity speed near the anode sheath, which for copper is around 13.2 kms^{-1}. For the experiments shown in this work with inter-electrode gaps of 1-9cm this equates to an ion particle time of flight (TOF) τ_L of around 0.76-6.8μs. Another timescale involved in these processes is the characteristic time for the ion charge state produced in the cathode spot process to relax to its quasi-steady-state value, τ_S. This has been found to be on the order of 50-100μs for copper.[24] If the current pulse discharge time, τ, meets the inequality $\tau \gg \tau_S \gg \tau_L$, a quasi steady state or vacuum arc takes place. If $\tau \ll \tau_L$ the discharge is considered to be the spark phase of a vacuum discharge (or fast pulse discharge). In the case that $\tau_S \geq \tau \geq \tau_L$ the discharge is considered to be a short pulse discharge where the plasma flow parameters correspond to instant changes in the discharge current and S_0.[17] However the cathode spot evolution is theorised to be a fractal process with a finite life time.[14] The surface area of the combined plasma jets will then depend on the total pulse duration. Equation 6 can be modified to take this into account:[17]

$$S_t = S_0 \frac{I_{arc}}{I_{spot}} \left(1 + \frac{t}{\tau_S}\right) \tag{7}$$

In the case of the PPT under study (which has a discharge frequency of 136 kHz) the characteristic time of a single pulse of the total discharge is found to be around 3.68μs. Therefore dependent on the time of flight of the particles through the inter-electrode gap the processes involved can either be thought as a short or fast pulse discharge. The modelling of a fast pulse discharge requires the inclusion of a full set of time dependant magnetohydrodynamic equations. The modelling of a short pulse can be completed with quasi steady state assumptions with only the time dependence of the surface area of the combined plasma jets to be considered, which considerably simplifies the problem. As such the model developed only considers short pulses and limits the model's validity to comparisons with experimental data with an inter-electrode gap of 1cm ($\tau_L \cong 0.76\mu$s) and 3cm ($\tau_L \cong 2.27\mu$s). The developed model for short pulses is invalid for distances larger than 5cm for the experimental data undertaken. However, despite this limitation in the model, developed PPTs are typically copper based electrodes with gap distances of around 3cm, meaning the model is applicable for evaluating within these parameters.

The flow model is based on the following assumptions:[25]

- The plasma flow originates from a single or closely grouped number of cathode spots rather than several individual plasma flows from spots located at distances far apart from each other.

- The discharge is a short pulse arc where quasi steady state can be assumed.
- It is assumed that the compression of the plasma flow by its own magnetic field is identical to the compression of the current flow, which has the same cross sectional area.
- The self generated magnetic field is stronger than the external magnetic field created by current flowing through the electrodes and is limited to a small region near the edge of the plasma column. Thus the self generated magnetic field shields the plasma contained within the column from external magnetic effects, i.e. The conductivity within the plasma column is unaffected by both external magnetic fields and self generated magnetic fields.
- The model uses a one dimensional system of equations which takes into account the plasma flow cross sectional area, $S(z) = \pi r^2$. It is assumed that across the cross sectional area the plasma temperature, electron density, ion velocity, ion charge state and the current density are uniform.
- Electron energy losses due to heat conduction are ignored compared to energy lost due to joule heating and electron-ion collisions.
- The ion pressure is neglected in comparison to the electron pressure given that the electron temperature is much greater than the ion temperature in the cathodic plasma.
- The plasma originates from material eroded by cathodic spot emission sites and these provide the initial boundary conditions of the plasma close to the cathode. All the mass eroded is assumed to be ionised particles and is accelerated within the plasma column. The introduction of neutral particles or particulates into the discharge gap from cooling emission sites on the cathode is ignored.
- The anode is considered a passive collector of the charge and mass which means that the model is only adequate within the inter-electrode gap outside of the anode sheath region. Additional effects on the anode (i.e. anodic spot creation) are neglected and the addition of these processes are left for future work.
- It is assumed that the electron temperature of the plasma flow is limited and is a function of the initial electron temperature in the cathode spot region.

In the following flow model, the z-axis is defined as the axis connecting the midpoint of the electrodes, the y-axis is defined as the axis aligned with the magnetic fields created by the current flow through the electrodes and the x-axis is defined as being perpendicular to z and y axis. In polar co-ordinates the z-axis is the same as the cartisian co-ordinates and the the r-axis is in the x-y plane.

The flow model is based on solving the following MHD equations in cylindrical coordinates for steady state. For the moving plasma the continuinity and momentum transfer equations are used:

$$\frac{\partial \rho}{\partial t} + \nabla \cdot (\rho V) = 0 \tag{8}$$

$$\rho \left(\frac{\partial}{\partial t} + V \cdot \nabla \right) V = J \times B - \nabla P \tag{9}$$

For the electrical current the conservation law is used:

$$\nabla \cdot J = 0 \tag{10}$$

For the self generated magnetic field Ampere's law is used:

$$\nabla \times B = \mu_0 J \tag{11}$$

In cylindrical coordinates for steady state these equations can be simplified to:[26]

$$\frac{1}{r} \frac{\partial}{\partial r} (r \rho V_r) + \frac{\partial}{\partial r} (\rho V_z) = 0 \tag{12}$$

$$\rho \left(V_r \frac{\partial V_z}{\partial r} + V_z \frac{\partial V_z}{\partial z} \right) = \frac{\partial P}{\partial z} + J_r B_\theta \tag{13}$$

$$\rho\left(V_r\frac{\partial V_r}{\partial r}+V_z\frac{\partial V_r}{\partial z}\right)=\frac{\partial P}{\partial r}-J_zB_\theta+J_\theta B_z \tag{14}$$

$$\frac{1}{r}\frac{\partial}{\partial r}\left(rJ_r\right)+\frac{\partial}{\partial r}\left(J_z\right)=0 \tag{15}$$

$$B_\theta=\frac{\mu_0}{r}\int_0^r J_z r dr \tag{16}$$

The plasma pressure within the flow is a combination of the ion temperature and the electron temperature given by the ideal gas law. However, due to the assumption that the electron temperature is much greater than the ion temperature, the contribution to the total pressure from the ion pressure can be neglected and the plasma pressure, P, becomes:

$$P\simeq k_B T_e N_e \tag{17}$$

The properties of electron temperature within the plasma flow are described by the electron heat balance equation:[27]

$$\frac{d}{dz}\left(\frac{3}{2}PV_eS\right)+P\frac{d}{dz}\left(V_eS\right)=\frac{I^2}{\sigma S}-Q_{ei}S \tag{18}$$

As the current is related to the velocity of a particle, a relationship can be established between the electron velocity, V_e, and the flow velocity:[27]

$$V_e=V_z\left(1+\frac{1}{\alpha_i}\right) \tag{19}$$

α_i is the ion current normalised by the arc current ratio and is explained further in the plasma mass model section.

The electrical conductivity is a measure on how easy it is for the current to flow through the plasma and is heavily dependent on the relative motion and collision frequencies between the ions and the electrons within the plasma. The conductivity is made from three elements; the conductivity that is parallel to the direction of the magnetic field, the conductivity that is perpendicular to the direction of the magnetic field and the conductivity due to relative motion around the magnetic field caused by the Hall effect. A tensor can be formed to describe the conductivity through the plasma:

$$\sigma=e_0\begin{bmatrix}\sigma_\perp & -\sigma_H & 0\\ \sigma_H & \sigma_\perp & 0\\ 0 & 0 & \sigma_\parallel\end{bmatrix} \tag{20}$$

Where the perpendicular, $\sigma_\perp$, Hall, σ_H, and parallel, $\sigma_\parallel$, conductivities are defined as:

$$\sigma_\perp=\frac{\omega_{pe}^2\left(\upsilon_{ie}-i\omega_{pulse}\right)}{\left(\upsilon_{ie}-i\omega_{pulse}\right)^2+\Omega_e^2}+\sum_i\frac{\omega_{pi}^2\left(\upsilon_{ie}-i\omega_{pulse}\right)}{\left(\upsilon_{ie}-i\omega_{pulse}\right)^2+\Omega_i^2} \tag{21}$$

$$\sigma_H=\frac{\omega_{pe}^2\Omega_e}{\left(\upsilon_{ie}-i\omega_{pulse}\right)^2+\Omega_e^2}+\sum_i\frac{\omega_{pi}^2\Omega_i}{\left(\upsilon_{ie}-i\omega_{pulse}\right)^2+\Omega_i^2} \tag{22}$$

$$\sigma_\parallel=\frac{\omega_{pe}^2}{\left(\upsilon_{ie}-i\omega_{pulse}\right)}+\sum_i\frac{\omega_{pi}^2}{\left(\upsilon_{ie}-i\omega_{pulse}\right)} \tag{23}$$

The plasma frequency, ω_p, of the particle species, j, is:

$$\omega_{pj}=\left(\frac{N_jQ_n^2e^2}{m_je_0}\right)^{\frac{1}{2}} \tag{24}$$

In the presence of a magnetic field the particles will begin to rotate around them at a given frequency. This frequency of gyration of the particle species, j, is:

$$\Omega_j = \frac{Q_n e B}{m_j} \tag{25}$$

It is assumed that the bulk of the plasma within the column is 'shielded' from the external magnetic fields by the self generated magnetic field, hence $\Omega_j = 0$. The frequency dependant effect on the collisional electron-ion frequency is only significant at high frequencies, in the typical range for PPT discharges this effect can be neglected, which simplifies Equations 21 and 23.

As the electron temperature of the plasma increases so does the collisional frequency of electrons and ions. This causes an increase in the plasma pressure but a decrease in the flow velocity of the plasma. Subsequently as the velocity decreases so does the cross sectional area of the plasma flow which in effect increases the electron density. The increase in the electron density further increases the plasma pressure in a runaway effect that causes the plasma flow to become 'stationary'. To limit this growth it is assumed that the electron temperature within the plasma flow cannot exceed a critical temperature, T_{cr}. The critical temperature is defined as:[28]

$$T_{cr} = \frac{75 M^2 T_m \overline{Q_0}}{192 \overline{Q}} \tag{26}$$

The Mach number for all plasma jets originating from a cathode surface is $\simeq 3.5$. The frequency at which the electrons and ions collide, υ_{ie}, is given as:[29]

$$\upsilon_{ie} = 3.62 \times 10^{-6} \frac{\Lambda N_e T_e^{-\frac{3}{2}}}{\overline{Q}} \tag{27}$$

Collisions within the plasma between the electrons and the ions can be considered as binary collisions. However, due to the relative masses, velocities and sizes, an electron is more likely to be scattered by a small amount due to the interaction of the coulomb forces between the particles rather than a larger deflection due to a direct impact between the particles. Due to the small scatter in a single collision event it is more advantageous to describe the effect of numerous small scatter events (as would be present in plasma) rather than describe the collisional processes by a direct collision. The coulomb logarithm, Λ, is the factor by which small-angle collisions are more effective than large-angle collisions. For the plasma conditions most typically found in a short duration vacuum arc the coulomb logarithm is described as:[29]

$$\Lambda = 23 - log\left(N_e^2 \overline{Q} T_e^{-\frac{3}{2}}\right) \tag{28}$$

From the ionisation levels of the plasma particle species and the electron temperature an approximation for the ion charge state distribution can be made. An approximate method using the Grizinski$\check{i}$ formula for the electron impact ionisation cross section of ions and averaging over the Maxwell electron velocity distribution is used to find the ionisation coefficient, $k_n(t)$, of the nth charge state level:[30]

$$k_n(t) = 1 \times 10^{-20} \left(\frac{8 k_B T_e}{\pi m_e}\right)^{\frac{1}{2}} \left(\frac{13.6e}{I_{i,n}}\right)^2 \exp\left(\frac{-I_{i,n}}{k_B T_e}\right) \tag{29}$$

Table 2 lists the energy required to raise the ion state from the n^{th} state to the $n^{th}+1$ state. The ionisation coefficient can be used to estimate the ratio of the number density of the n^{th} charge state to the total number of ions present in the plasma. This is known as the charge state fraction and can be found along the plasma flow using:[17]

$$f_n(z) = C_n \left(\frac{(-z - z_0)\, k_{n+1} N_e}{V_z}\right) - C_{n-1} \left(\frac{(-z - z_0)\, k_n N_e}{V_z}\right) \tag{30}$$

where C_n is a function of the charge state fraction distribution f_n^0 at the freezing zone of the cathode spot, see Table 1, and is expressed as:

$$C_n = \sum_{n=1} f_n^0 \tag{31}$$

The mean ion charge state along the cathode-anode axis is the sum of the charge state fraction distribution along the axis:

Table 2. Energy required to raise ion state

Ion	Energy, eV	Ion	Energy, eV	Ion	Energy, eV
Cu	7.73	Cu^{+10}	33.30	Cu^{+20}	107
Cu^{+1}	12.57	Cu^{+11}	103.70	Cu^{+21}	112
Cu^{+2}	16.55	Cu^{+12}	32.00	Cu^{+22}	144
Cu^{+3}	20.54	Cu^{+13}	34.00	Cu^{+23}	122
Cu^{+4}	22.42	Cu^{+14}	49.00	Cu^{+24}	126
Cu^{+5}	23.20	Cu^{+15}	36.00	Cu^{+25}	170
Cu^{+6}	36.00	Cu^{+16}	37.00	Cu^{+26}	109.50
Cu^{+7}	27.00	Cu^{+17}	76.00	Cu^{+27}	8474.88
Cu^{+8}	33.00	Cu^{+18}	37.59	Cu^{+28}	505.24
Cu^{+9}	33.00	Cu^{+19}	1026.41	Cu^{+29}	N/A

$$\overline{Q}(z) = \sum_{n=1} Q_n f_n(z) \tag{32}$$

The electron density, which is a function of the arc current, can be calculated from:[27]

$$J_i = J_e \alpha_i \rightarrow \overline{Q} e N_i V_z = \alpha_i \frac{I}{S} \rightarrow N_e = \frac{I \alpha_i}{e S V_z} \tag{33}$$

Assuming quasi-state neutrality the ion density is thus, $N_i = \frac{N_e}{\overline{Q}}$. Finally the rate of energy loss for the ionisation of ions is defined by the the expression:[31]

$$Q_{ie} = N_e N_i \sum_{n=1} I_{i,n+1} k_{n+1} f_n \tag{34}$$

Equations 12 to 34 can be used to simulate the conditions of the plasma in the quasi-steady state plasma flow between the electrodes by solving a differential set of equations. By expanding out the heat balance equation (Equation 18) to obtain an expression for $\frac{dT_e}{dr}$ this can then be joined with the following set of equations that were obtained from Equations 12 to 16 and 33:[26]

$$\frac{d\left(\rho V_z S\right)}{dz} = 0 \tag{35}$$

$$\frac{dS}{dz} = 2\pi R \frac{V_r}{V_z} \tag{36}$$

$$\frac{dR}{dz} = \frac{V_r}{V_z} \tag{37}$$

$$\left(\rho V_z S\right) \frac{dV_z}{dz} = -\frac{d\left(PS\right)}{dz} \tag{38}$$

$$\left(\rho V_r S\right) \frac{dV_z}{dz} = \frac{3PS}{R} - \frac{\mu_0 I^2}{2\pi R} \tag{39}$$

$$\frac{dN_e}{dz} = \frac{I \alpha_i}{e S^2 V_z^2} \frac{dS}{dz} \frac{dV_z}{dz} \tag{40}$$

This system of equations was solved using the Matlab ODE23 differential equation solver, given an initial flow area from Equation 7 and a given arc current. The initial values of the boundary conditions for the set of equations is summarised in Table 1 and 3.

Table 3. Boundary conditions for the plasma flow model

Boundary condition	Value
$(\rho V_z S)$	$\Gamma_i I$
S_0	Equation 7
R_0	$\sqrt{\frac{S_0}{\pi}}$
V_{z0}	13.2kms^{-1}
V_{r0}	0
T_e	11605 K
N_e	$\frac{I\alpha_i}{eS_0V_z}$

From the flow model the parameters of the plasma along the flow axis from cathode to anode can be established. The resistance of the plasma flow can be found from the inverse of the conductivity integrated across the distance between the electrodes:

$$R_{plasmaflow} = \int_0^h \frac{1}{\sigma(z)} dz \tag{41}$$

The plasma flow resitance however is minimal compared to the effective resistance seen across the voltage drop in the sheath regions. Plasma is 'insulated' from the environment that surrounds it by the natural sheaths that are created whenever plasma interacts with a surface. The sheath is a dynamic entity with a structure and thickness that depends on the potential difference between the solid surface and the plasma potential.

In the cathode spot creation process the introduction of charge and mass via emission sites circumnavigates the effect of the cathode sheath. However, the anode sheath needs closer attention. When the potential of the solid surface rapidly changes (as it does in the PPT), the change in the electric field causes the electrons to leave immediately whilst the slower heavier ions remain 'fixed' for a small instance. This type of sheath is known as the ion matrix sheath and the thickness of such a sheath is:

$$d_{sheath} = \sqrt{-\Phi_{wall}\frac{2e_0}{eN_i}} \tag{42}$$

The Child-Langmuir Law describes how the species current is effected by the sheath. It states that the current per unit area which can pass through a planar sheath is limited by space-charge effects. We have assumed by invoking the ion matrix sheath that the ion current is negligible and so the limited arc current becomes:

$$J_{e-sheath} = \frac{I_{e-sheath}}{S_{anode}} = \frac{4e_0}{9}\left(\frac{2e}{me}\right)^{\frac{1}{2}}\frac{\Phi_{wall}^2}{d_{sheath}} \tag{43}$$

The lumped circuit analysis model is used to calculate Φ_{wall} at any given time, whilst the flow model is used to calculate N_i and S_{anode} near the anode. The limitation in the arc current by space-charge effects can be considered as a pseudo resistance for the purposes of the lumped circuit analysis model. Using Ohm's law, the limited arc current and the potential difference between the sheath and the sheath wall (which is $\simeq \Phi_{wall}$ if the plasma potential is relatively small), then combining with Equation 41, the total plasma resistance becomes:

$$R_{plasma} = R_{sheath} + R_{plasmaflow} \simeq \frac{V_{sheath}}{I_{e-sheath}} \tag{44}$$

E. Electrode Errosion Model

The properties of a cathode spot, in which the plasma mass originates, is only dependant on the material the cathode spot is formed on. For the same material one cathode spot compared to another are remarkably similar. This has allowed experimentalists to form certain parameters for many metals, which include the

ion normalised by arc current, α_i, which is used to describe the ratio between the ion current and the arc current in a cathodic plasma, see Figure 10. This has a value of $\alpha_i = 0.114$ for copper. Another parameter is, Γ_i, the ion erosion rate, which describes the total ion mass eroded from the electrode surface per unit charge. For copper this value is $33.4\mu\text{gC}^{-1}$. This can be used to determine the rate of mass loss from the electrode surface as a function of the discharge current:

$$\frac{dm}{dt} = \frac{dm}{dQ}\frac{dQ}{dt} \Rightarrow \Gamma_i I \tag{45}$$

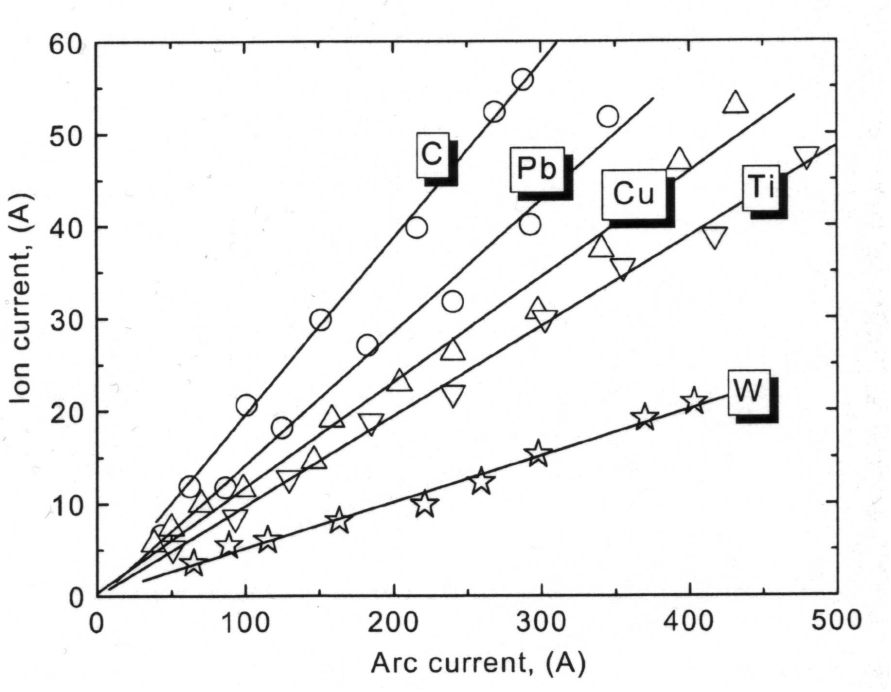

Figure 10. Ion current as a function of arc current for different cathode materials[32]

The total mass eroded from the electrodes, if experimentally measured, should be higher than found from Equation 45 due to macro particulate and neutral particle ejection that are produced from the cathode crater as it cools down after it has 'exploded'. Macro particulates are accelerated at a slower rate than the plasma ions and electrons due to their increased mass and so their effect on the dynamics of the plasma flow is neglected.

Neutrals are neglected for a PPT without Teflon^{TM} as there is no significant source of neutrals during the cathode spot process because most of the particles are ions. For copper the mean ion charge state is Cu^{2+} (72.1% of the total population).[14] In addition neutrals occurring from cooling emission sites are formed on timescales longer than the discharge process and so are assumed not to interact or effect the discharging plasma.

F. Force Model

During the PPT discharge only the Lorentz force acting upon the 'plasma flow' to move the flow as a bulk system in the direction of the nozzle exit is considered. If Teflon^{TM} was present the flow model would have to account for the additional mass from the Teflon^{TM} and the subsequent neutral particle sheet from the Teflon^{TM} surface. The neutral sheet is not accelerated by electromagnetic forces but would expand out of the nozzle under thermal expansion.

It was noted in literature that the location of the neutral particle sheet above the cathode (when Teflon^{TM} was involved) was also the location where the next luminous activity (cathode emission site) would occur when the current through the current loop reversed direction.[33] This would make sense, as the neutral particle sheet (if excited and ionised) would act as a bridge of least resistance between the two electrodes

where current could flow. This would promote an area of ion bombardment on the rough cathode surface where an emission site would form. After the initial discharge across the Teflon^{TM} surface, further pulses would begin from the formed neutral sheet at a location specified by the dynamics of the neutral sheet.

In the case of this work where Teflon^{TM} is not present, a neutral particle sheet is thought not to form. Instead, the formation of each new plasma sheet is assumed to be in a location where the circuit resistance is minimal (i.e. where $R_{electrodes}$ is small). This is usually at the closest point to the capacitor, but still within the discharge chamber.

When calculating the Lorentz force between the plasma flow and the magnetic field that is set up around the electrodes, a magnetic field distribution based on two infinitely long copper wires was assumed. The magnetic field distribution was calculated along the axis between the wires. This magnetic field distribution along the axis between the two electrodes was assumed to be similar to a magnetic field around rectangular electrodes, so that across the width of the rectangular electrodes the distribution was assumed to be constant and fringe effects were ignored. The accuracy of this magnetic field distribution is unknown and further work is required to confirm its applicability.

Using the Lorentz force evaluated over the entire plasma flow volume, Newton's second law and Equation (45) leads to an expression for the acceleration of the plasma bulk as a whole out of the thruster nozzle;

$$\Gamma_i I \frac{dx}{dt} + \frac{dx^2}{d^2t}\Gamma_i \int_0^t I dt = \int_V (J \times B)\, dV \tag{46}$$

Whilst evaluating the Lorentz force the magnetic field contribution from the self induced magnetic field in the x-y plane will cancel itself out and so only the external magnetic field in the y-axis needs to be considered. The external magnetic field in the x-axis and the z-axis is zero as fringe effects are neglected. The current density in the x-y plane is also zero. The Lorentz force integrated over cylindrical co-ordinates is therefore:

$$\int_V (J \times B)\, dV = \int_V \frac{I_z}{\pi R^2(z)} \left(\frac{\mu_0 I_z}{2\pi(z+\phi)} + \frac{\mu_0 I_z}{2\pi(h-z+\phi)} \right) dV = \frac{\mu_0 I_z}{2\pi} log \frac{2h}{\phi + h} \tag{47}$$

where ϕ is half the electrode thickness.

G. Complete PPT Discharge Model

The model implementation used the Matlab dde23 delayed differential equation solver. The toolset of this solver allows 'events' to be set that, if obtained, would terminate the solver. Parameters can then be altered and the solver restarted using the terminated solution and altered parameters to become the new boundary conditions and 'history' for the next pulse. The solver is also capable of providing an estimate of the $\frac{dL_{circuit}}{dt}$ by using the time lag function of the solver with the assumption that:

$$\frac{\Delta L}{\Delta t} \Rightarrow \frac{dL}{dt} \tag{48}$$

where the time lag was set sufficiently small at 0.1μs. Equations (2), (45), (47) and (48) can be rewritten in state space and solved as a set of simultaneous equations:

$$\begin{aligned}
\dot{x(1)} &= x(3) \\
\dot{x(2)} &= x(4) \\
\dot{x(3)} &= \frac{\frac{\mu_0 I_z}{2\pi} log \frac{2h}{\phi+h} - x(3)x(4)\Gamma_i}{x(6)} \\
\dot{x(4)} &= \frac{V_0 - \frac{x(2)}{C_{PPT}} - x(4)\dot{x(5)} - x(4)R_{circuit}}{L_{circuit}} \\
\dot{x(5)} &= \frac{L_{circuit} - L_{circuit-lag}}{1 \times 10^{-7}} \\
\dot{x(6)} &= \Gamma_i x(4)
\end{aligned} \tag{49}$$

When the integral of the current, $\dot{x(2)}$, reached either a maximum or minimum (i.e. zero current) the dde23 solver would pause. It was at this stage experimental observations suggested that a new plasma

bulk would be created and accelerated out of the PPT. So the distance travelled by the plasma bulk, x(1), the plasma bulk speed, x(3) and the plasma bulk mass, x(6), were reset to their initial conditions and the other values remained unaltered. The dde23 solver was then restarted. The initial conditions for the set of differential equations is shown in Table 4. The initial conditions were arbitrarily chosen to be relatively small but non-zero values.

Table 4. Boundary conditions for the lumped circuit analysis model

Boundary condition	Value
$x(1)$	0.1 mm
$x(2)$	0
$x(3)$	1 mms^{-1}
$x(4)$	10 A
$x(5)$	0
$x(6)$	0.001 μg

There are processes that are not modelled within the lumped circuit analysis which may also affect the plasma bulk properties. The accuracy of the magnetic field distribution has a significant role in determining the Lorentz force which in turn determines the bulk plasma speed. If the bulk speed is 'slow' when the current in the circuit loop reverses, there may still be a previous plasma bulk in the discharge channel. In reality the circuit would then be closed by that plasma bulk and the discharge would carry on from wherever the plasma bulk might be at that time. However, in the model it is assumed a new sheet is initiated and so it is possible to have two or more plasma bulks occurring in the same discharge channel. If the bulk speed is 'fast' and the bulk plasma has left the discharge chamber before the current reverses then multiple plasma bulks cannot occur.

The effect of the plasma bulk canting is also not taken into consideration as it is beyond this simplified model. It is theorised that the canting effect originates from the vectored velocity between the plasma flow (which is in the direction of the anode) and the velocity of the plasma bulk (which is in the direction of the nozzle and is a function of the Lorentz force). The two combined create a vectored plasma bulk velocity. By applying diverging electrodes to the PPT the vectored velocity can be realigned with the axis in which the nozzle is in to increase performance. From the frame of reference of the ion motion within the plasma flow the canting will cause the accelerated ion to experience an off axis electric field which may alter the properties of the plasma flow. Incorporating these processes is left for future work.

III. Model Validation

The model was validated against experimental results by comparing the predicted current profile with the experimentally observed current profile. The radius of an individual cathode spot has been shown to expand between 1-2mm in the first 10ns, see Figure 9. On timescales greater than this no references of the radius of the cathode spot for high current discharges were found. The properties of the plasma flow at the anode sheath are a function of the initial flow area (which is a function of the individual cathode spot area). By comparing the predicted current profile with experimental results (in the quasi steady state assumption range i.e. below 3cm) for individual cathode spot radii from 0.5mm to 4.5mm, a best fit match was found, see Figure 11. For the 1cm gap distance the 1.5mm and 2.5mm radii under-predicted the current profile, whilst for the 3cm gap distance the 0.5mm and 4.5mm radii under-predicted the current profile. By a process of elimination a cathode spot radius of 3.5mm was found to best fit the data sets. This value was then fixed when comparing all other data sets.

Further optimisation of the radius of the individual cathode spot is left for future work as it requires the modelling of anode spot processes in the flow model and a more accurate value for the capacitor inductance and resistance in the lumped circuit analysis model.

Figure 12 shows the validity of the model to predict the current profile at 1443V discharge at an electrode gap separation of 3cm. The comparison shows two features that are not modelled accurately. The first is that the current peak from the experimental results and the modelled results are artificially placed in line with each other. This is because the model does not predict the occurrence of the exponential increase in the

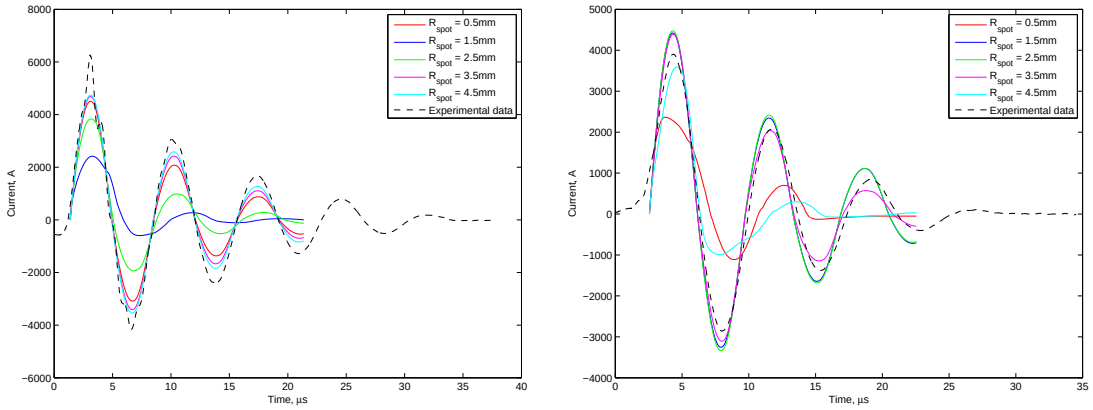

Figure 11. Optimisation of R_{spot} by creating a best fit between the predicted and experimentally observed current profiles at 1cm (Left) and 3cm (Right) electrode separation

current waveform seen in the first few microseconds of the experimental data. This physical phenomenon is thought to be from the discharge gap breakdown mechanism, which is not modelled.

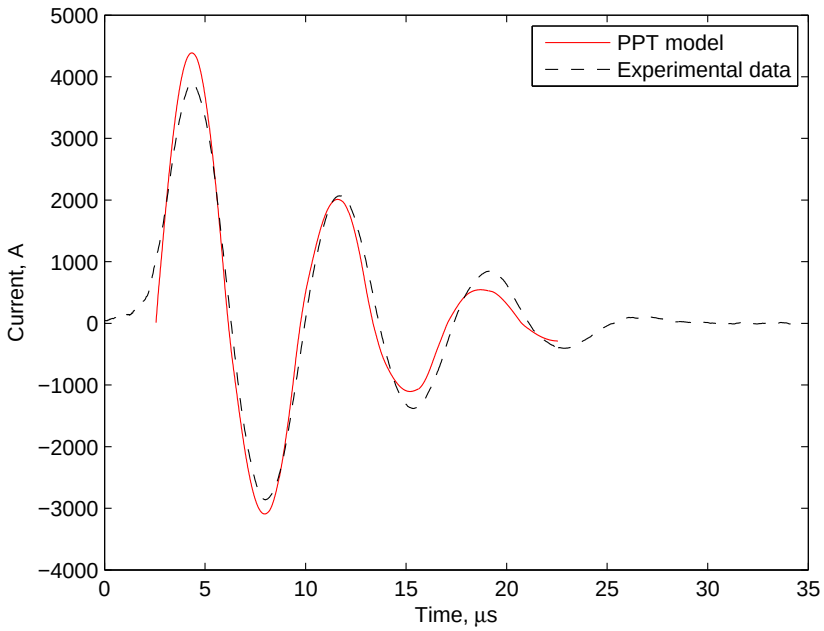

Figure 12. Comparison of the predicted and experimentally observed current profiles at 1443V and 3cm electrode separation

The second feature is the over prediction of the current pulse in the first peak. This may be linked to the breakdown mechanism or it may also be linked to the possible inaccuracy in the simplified model of how the cathode spot radius changes with time (Equation 7). Figure 13 compares the validity of the model over a range of experimental measurements from 748V to 2493V at a discharge gap of 3cm.

In context with the previous observations Figure 13 generally shows good correlation between the predicted and observed current profiles. Figure 14 compares the validity of the model over a range of experimental measurements from 770V to 2600V at a discharge gap of 1cm.

Figure 14 shows a reasonable correlation between the predicted and modelled data. However, as the discharge voltage is increased the model increasingly under-predicts the current profile. This is thought to be because the model does not take into account anode spot creation processes, which is thought to be the

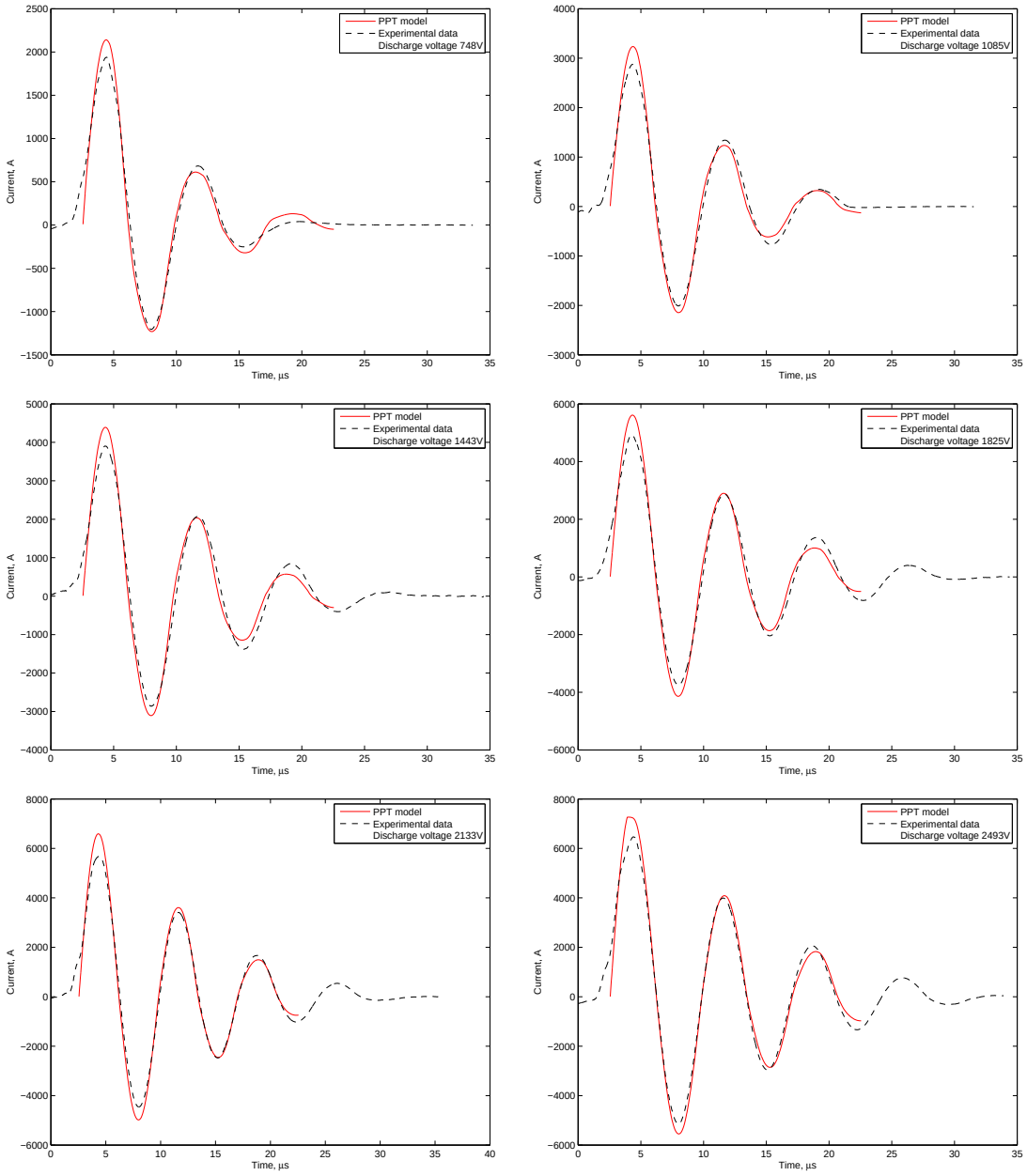

Figure 13. The modelled current (red) compared to experimentally obtained current measurements (black dash) for discharges between 748V and 2493V at an electrode separation distance of 3cm

cause of the visible spikes seen in the first (and sometimes second) peaks of the experimental data curves.

Figure 15 shows that the peak plasma bulk speed for a 1443V discharge at a 3cm electrode separation distance is just under 12kms^{-1}. A selection of peak ion speed velocities measured in literature, with time of flight probes are: 26-40kms^{-1},[34] 4-15kms^{-1}[35] and 15.5-35kms^{-1}.[13] The model predicts the range of peak ion velocities for 1cm and 3cm between 748V and 2600V discharges to be 3.5-22kms^{-1}. This range predicted by the model is within the order of magnitude from literature but future work and experiments will be required to measure the peak ion speeds exactly with a time of flight probe. The accuracy of the Lorentz force model will depend significantly on the accuracy of the magnetic field distribution model.

Within the limited parameters to validate the compiled model with experimental values, the model has been shown to give relatively accurate results for the discharge current profiles over a range of discharge parameters, as long as they remain within the boundaries of the quasi steady state assumption. The model

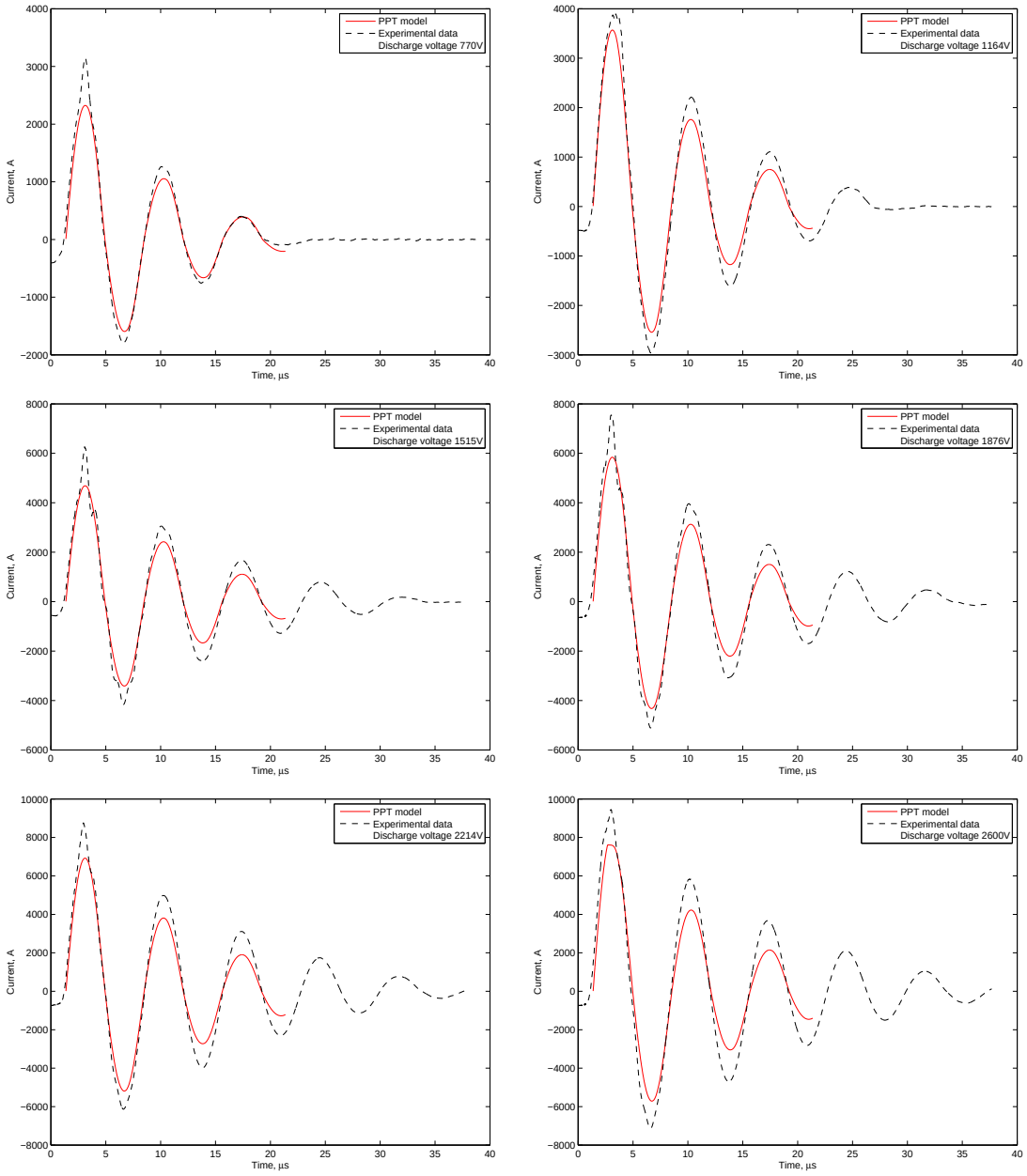

Figure 14. The modelled current (red) compared to experimentally obtained current measurements (black dash) for 770V and 2600V discharges at an electrode separation distance of 1cm

also provides a relative good match between predicted and experimentally observed peak ion speed velocities.

IV. PPT Analysis

The completed model can be used to investigate the internal plasma processes of the PPT and possibly highlights features that have been seen in experimental literature but unexplained in theory. The analysis will look at the properties of the plasma flow, assumed to be in quasi steady state, across the electrode discharge gap and how the quasi steady state plasma properties change over the discharge time. For the analysis of the plasma the model was set up with the parameters given in Table 5.

Figure 16 shows the current profile of the first pulse. The times of interest are at 0.05μs, 0.70μs and 1.75μs, which represent the start of the pulse, halfway through the pulse rise and the peak of the current

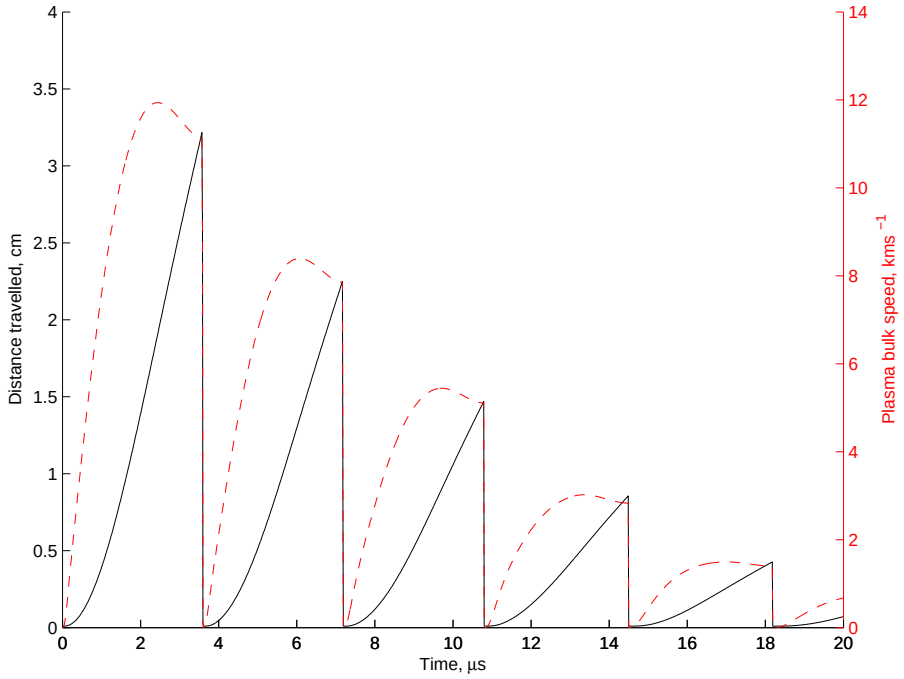

Figure 15. The bulk plasma speed accelerated by the $J \times B$ product for a 1443V discharge at a 3cm electrode separation distance. Dashed: Plasma bulk speed, Solid: Distance travelled

pulse respectively.

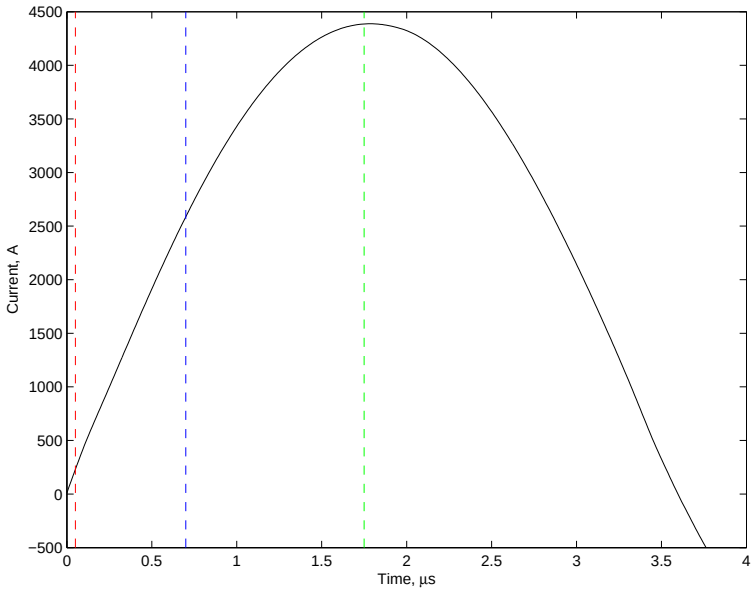

Figure 16. Predicted current profile of the first pulse discharge showing the relative current values at the analysis times of 0.05μs (red), 0.70μs (blue) and 1.75μs (green)

The flow radius distribution of the plasma flow between the electrodes at these times is shown in Figure 17, with the addition of a plot to show how the flow radius varies over the complete discharge.

At 0.05μs and 235A, the flow radius shows a conical like expansion that starts at 2-3 mm from the cathode surface. Before this the flow radius is relatively constant at approximately 1mm but during the conical expansion of the flow area this increases to approximately 12mm close to the anode surface. As the

Table 5. Parameters of the modelled PPT

PPT Parameter	Value
High Voltage Capacitor	
Capacitance	4.06μF
Charging voltage	1443V
Cap. Inductance	310nH
Cap. Resistance	33mΩ
Electrodes	
Setup	Parallel bar
Material	Copper
Width	20mm
Thickness	10mm
Discharge channel length	60mm
Separation	30mm

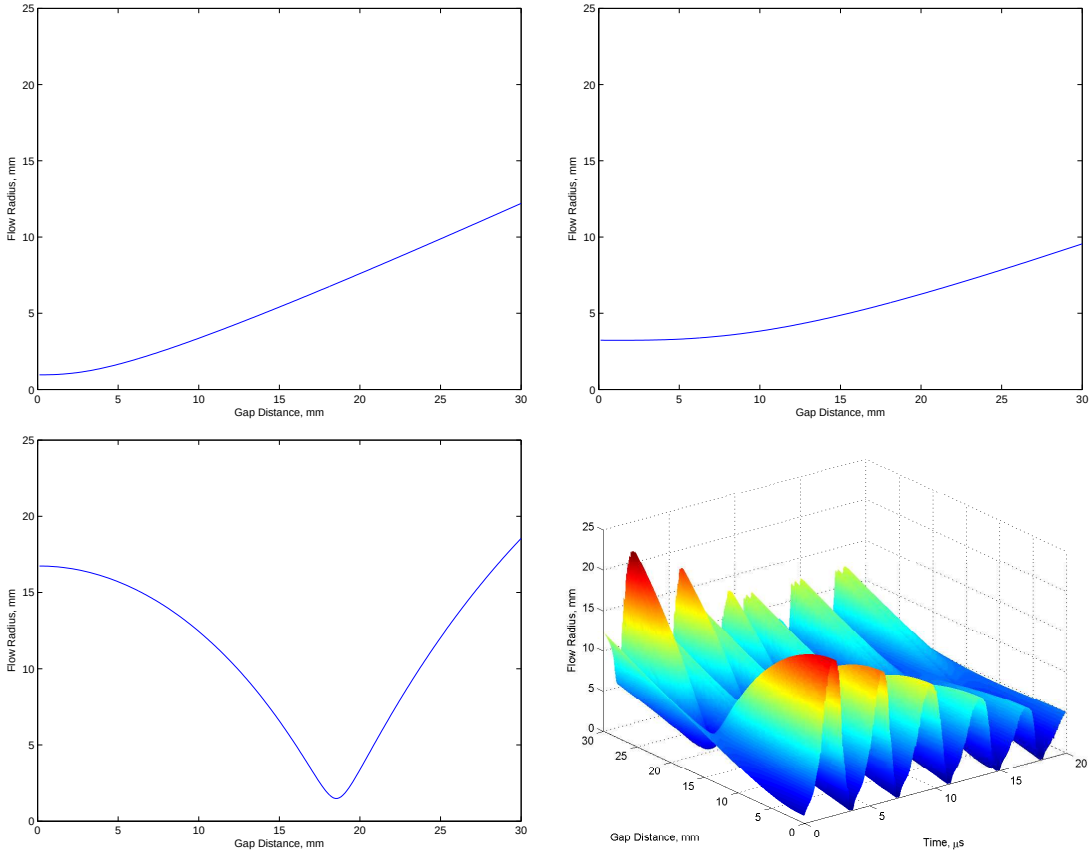

Figure 17. Predicted flow radius, Top left: 0.05μs, Top Right: 0.70μs Bottom Left: 1.75μs Bottom Right: Complete discharge

current rises to 2800A at 0.70μs the flow radius distribution looks similar, however the initial flow radius has increased to approximately 3mm. The start of the conical expansion has shifted to approximately 5mm. The radius of the flow at the anode has also decreased to approximately 9-10mm. A 3D representation of the plasma flow at 0.70μs can be seen in Figure 18.

As the current approaches the peak current of 4330A at 1.75μs a 'choke' formation is seen around 18-19mm from the cathode. In addition to this the initial flow radius has significantly increased to approximately

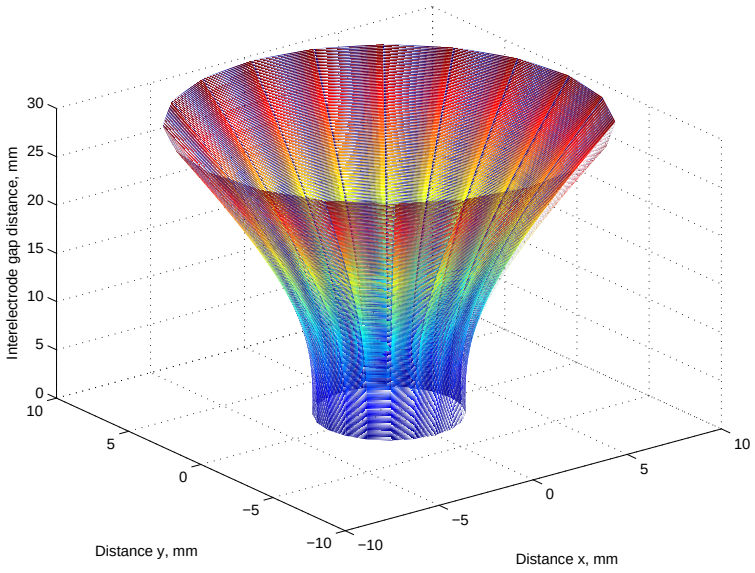

Figure 18. 3D representation of the plasma flow at 0.70μs

17mm. This is expected as the number of cathode spots increases with the discharge current. However, due to the change of dynamics of the flow caused by the choke, instead of the flow radius decreasing as the initial radius increases, (as seen from 0.05μs to 0.70μs), here the flow radius seems to have increased once again to approximately 18mm. The flow radius over the whole discharge shows that as the discharge progresses the 'choke' remains at the same distance from the cathode surface. Further modelling has shown that this is the case for all electrode geometries tested and in cases where the internal conductivity of the plasma column is unaffected by internal magnetic fields. In the absence of internal magnetic fields this 'choke distance' could be thought of as a material property of the electrode itself. The 'choke' has an effect on all the other plasma flow parameters.

At 0.05μs and 235A, the electron temperature shows a peak of 2eV at around 2.5mm from the cathode. The distribution initially rises rapidly to its peak and then gradually decays. At the anode the electron temperature has dropped to around 0.8eV. As the current rises to 2800A at 0.70μs the distribution looks similar although the peak temperature has risen to 5eV and the peak has shifted away from the cathode to approximately 9-10mm.

As the current approaches the peak current of 4330A at 1.75μs a new feature is observed and is attributed to the choke in the plasma flow. At the location of the choke the electron temperature sharply increases to approximately 200eV. Further modelling has shown that the magnitude of the peak temperature within the choke is a proportional function of the discharge current. The rise in the electron temperature is also linked with the electron density, see Figure 20.

The electron density in several respects shows similar relationships in time with the electron temperature. Figure 20 shows that as the plasma flow is restricted by the choke the electron density increases. As well as increasing due to the physical volume within the choke being small compared to the rest of the flow, the electron density also increases due to a secondary effect. As the plasma flow is constricted, the electron temperature significantly increases and further ionisation of the copper ions within the flow occurs. At the extreme temperatures mean ion charge states of Cu^{+25} are predicted, see Figure 21. The additional influx of electrons from the highly ionised copper particles adds to the total electron density.

The high ion charge states that are predicted to form in the choke by the model have been observed in literature. Figure 22 shows the ion signals for a 2kV discharge with a 2μF at 40nH capacitor.[36] It can be seen from the signal data that the ions with the highest ion charge state are observed first and as time progresses the ion charge state number decays. Plotting the decay of the ion charge state from the signal probe shows that with crude interpolation the ion charge state when the cathode spot was created predicted by the model is reasonable compared to the experimental results in the avaliable literature.

The ion charge state, electron temperature and electron density have a significant impact on the electron-ion collisional frequency and the plasma frequencies of the different species of particles. In turn these

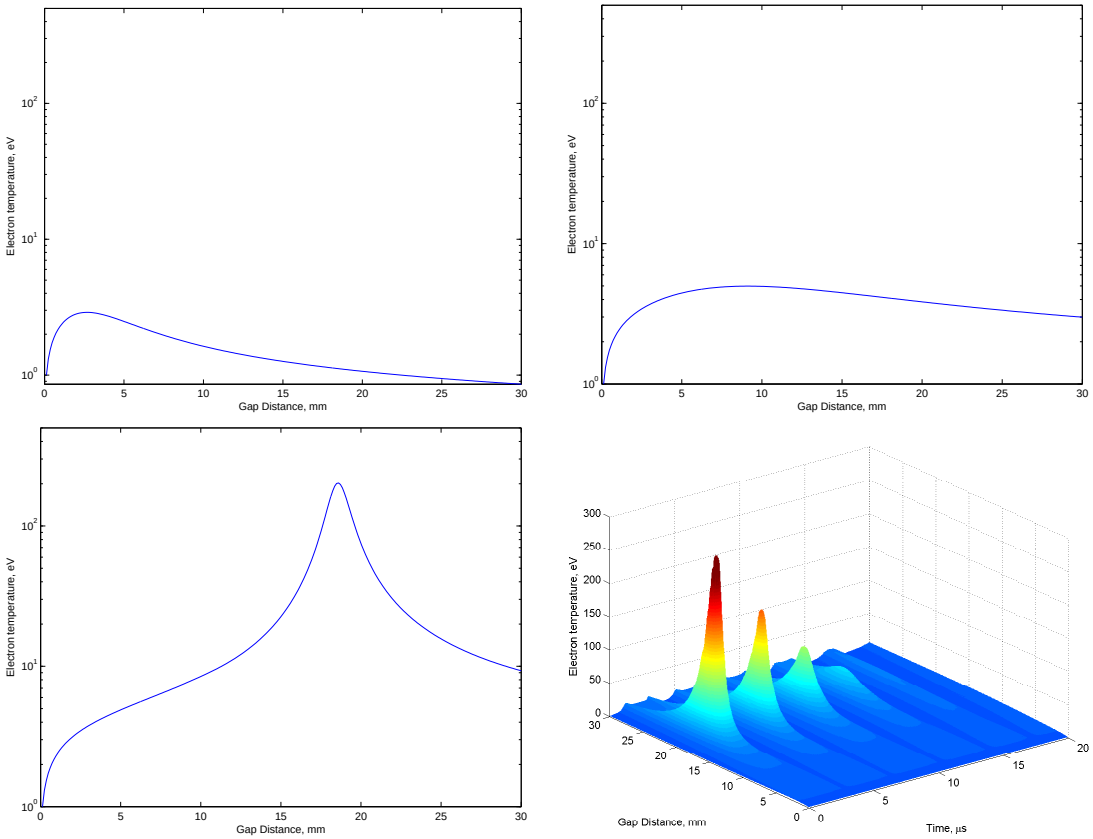

Figure 19. Predicted electron temperature, Top left: 0.05μs, Top Right: 0.70μs Bottom Left: 1.75μs Bottom Right: Complete discharge

distributions affect the conductivity of the plasma as depicted in Figure 23 for the complete discharge.

The plot shows some interesting features; foremost that the plasma flow conductivity is not constant across the discharge gap. Close to the cathode the conductivity is at its lowest and hence plasma resistivity is at its highest. When a moderate current is flowing through the plasma flow the conductivity increases rapidly to a peak as the ion charge state also rises. However this rise in conductivity is limited and after a threshold current the conductivity falls to a steady state for the majority of the pulse and for a majority of the discharge gap. As the discharge continues the location of the peak conductivity centres, traverses towards the choke point in the plasma flow (around 20mm).

The plasma resistance is small compared to the space-charge limiting effect of the anode sheath. The total circuit resistance and inductance is shown in Figure 24. The spikes in the plasma resistance are the locations where the current tends to zero and should be taken with caution. It has been observed in the literature that even as the discharge current tends to zero, a small amount of activity can still be seen within the discharge chamber, which in effect will limit the spike seen in the modelled data.[33] The profile of the circuit resistance shows that the resistance varies inversely with the current (which is to be expected), between 33mΩ to around 400mΩ. Also at the peak of the discharge current, the resistance of the plasma and sheath drops significantly and the total circuit resistance is only limited by the capacitor resistance.

The model has predicted that within the PPT discharge gap a choke point forms due to instabilities of the plasma flow which in turn causes a pinch effect. The dynamics of the choke significantly increases the electron density, the electron temperature and the mean ion charge state of the inter-electrode plasma.

V. PPT Optimisation

The flow model has been able to predict the current profile reasonably compared to experimental results. The accuracy of the model in estimating the Lorentz force is less well known. Without experimental time of

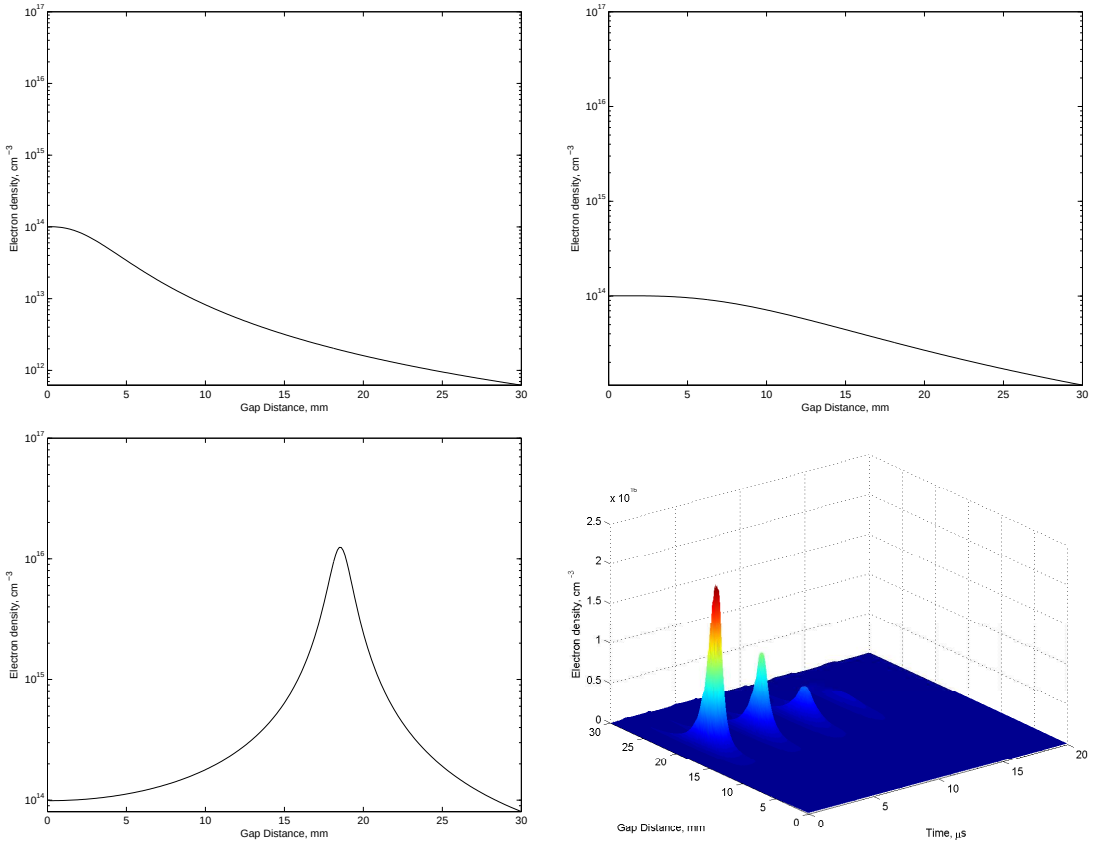

Figure 20. Predicted electron density, Top left: 0.05μs, Top Right: 0.70μs Bottom Left: 1.75μs Bottom Right: Complete discharge

flight data to verify the relative ion speeds it is difficult to be confident in the accuracy of the force model. However, the Lorentz force is a product of the magnetic field and the current density. The current density as predicted by the flow model fits experimental data well. The magnetic fields produced in the discharge are a proportional function of the current. Therefore even if the specific values of the magnetic field distribution are not entirely accurate, it can still be used to discover performance trends.

During the formulation of the Lorentz force model the magnetic field distribution was altered in different ways, including a draft model based on a rectangular bar electrode. However as seen in Figure 4, the current distribution within the electrode was not even due to the skin effect. This added additional complications and with limited computational resources meant the mapping of the magnetic field was left for future work.

As expected the predicted bulk plasma speed was significantly dependant on the field distribution, however the overall current profile was hardly affected. This lack of coupling is because $L_{Capacitor} \gg L_{electrode}$ and $R_{Capacitor} \gg R_{electrode}$, so the change in the effective electrode length within the closed circuit as the plasma propagated through the discharge channel had little overall impact. As part of the optimisation work the capacitor resistance and inductance will be lowered and so the coupling effect will become stronger. As this occurs, confidence in the results will lower, however the trends seen should show some insight into developing an optimised PPT.

Due to the approach used in this work many of the variables that are usually loosely defined in other models have been set by; the material properties of the electrode, the dynamics of the cathode spot process or negated by the removal of the Teflon^{TM} propellant. The changeable variables are physical values, variables set by real electrical components and the electrical characteristics of the capacitor. Here these are the dimensions of the parallel bar electrodes, the inductance, capacitance and resistance of the high voltage PPT capacitor and the voltage the capacitor is charged to. The electrode material could also be changed to other metal types, e.g. Aluminium, Carbon or Titanium. However, to obtain a full set of input parameters (conductivity, ionisation energies, plasma jet parameters etc) for each of the metals proved difficult. There

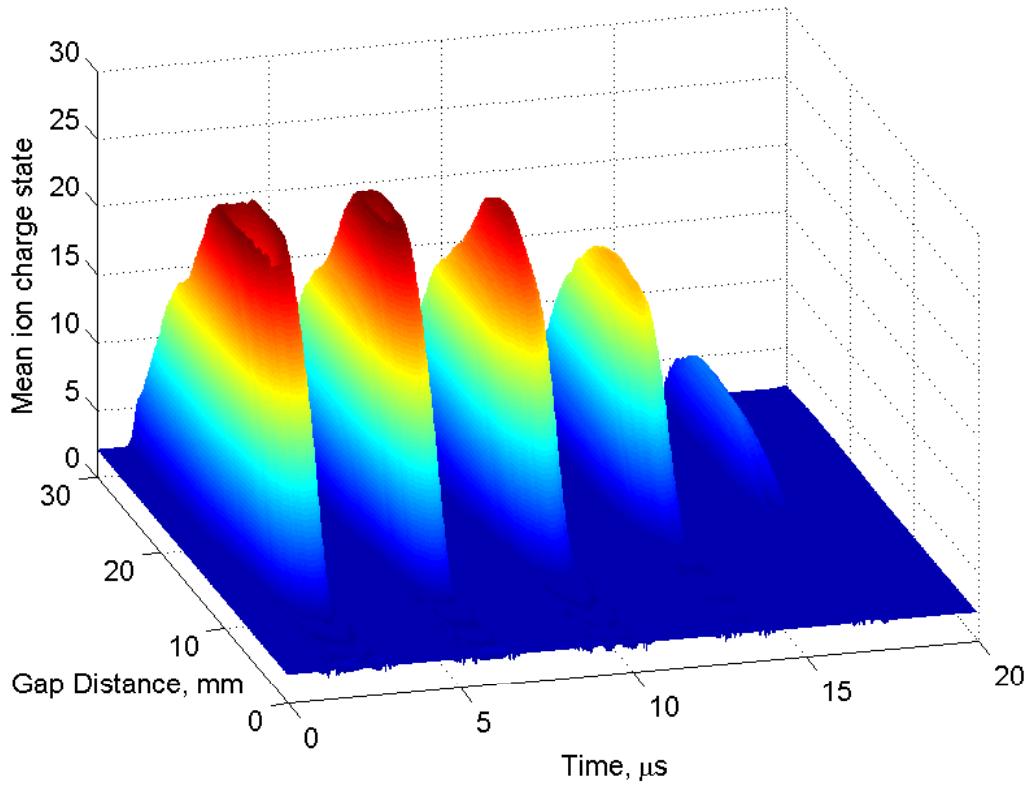

Figure 21. Predicted mean ion charge state for the complete discharge

was a necessity to ensure the correct cathode spot radius was used for the specific metal, which the flow model is very sensitive to. Both factors combined meant that this part of the optimisation was left for future work.

To optimise the performance of the PPT it is necessary to focus on two areas. The first is to increase the efficiency of converting electrical energy provided by the capacitor into kinetic energy to accelerate the bulk plasma. The second area is to maximise the impulsive force provided by the discharge, whilst keeping the material mass loss per discharge as low as possible. This will ensure the electrodes will last longer and so the PPT will be able to provide a larger total impulse. By varying the electrode geometry and the capacitor parameters it will be seen if this can be achieved.

The specific criteria looked at will be: the specific impulse, I_{sp}, the impulse bit, I_{bit}, the mass bit, m_{bit} and the efficiency of converting electrical energy into kinetic energy, η_{PPT}. The specific impulse, I_{sp}, is a measure of the thrust to the rate of use of propellant by sea level weight for any engine:

$$I_{sp} = \frac{\frac{dm}{dt}u_e}{\frac{dm}{dt}g_0} = \frac{u_e}{g_0} \tag{50}$$

The impulse bit, I_{sp}, is a measure of the momentum transferred by the engine in a short period of time. For the PPT this is the total Lorentz force (ignoring contributions from neutral particle gas and macro particulate dynamics) over the bulk volume for the complete discharge:

$$I_{bit} = mu_e = \int_{t_0}^{t_f} \int_V J \times B dV dt \tag{51}$$

The mass bit is found by integrating Equation 45:

$$m_{bit} = \int_{t_0}^{t_f} \Gamma_i I dt \tag{52}$$

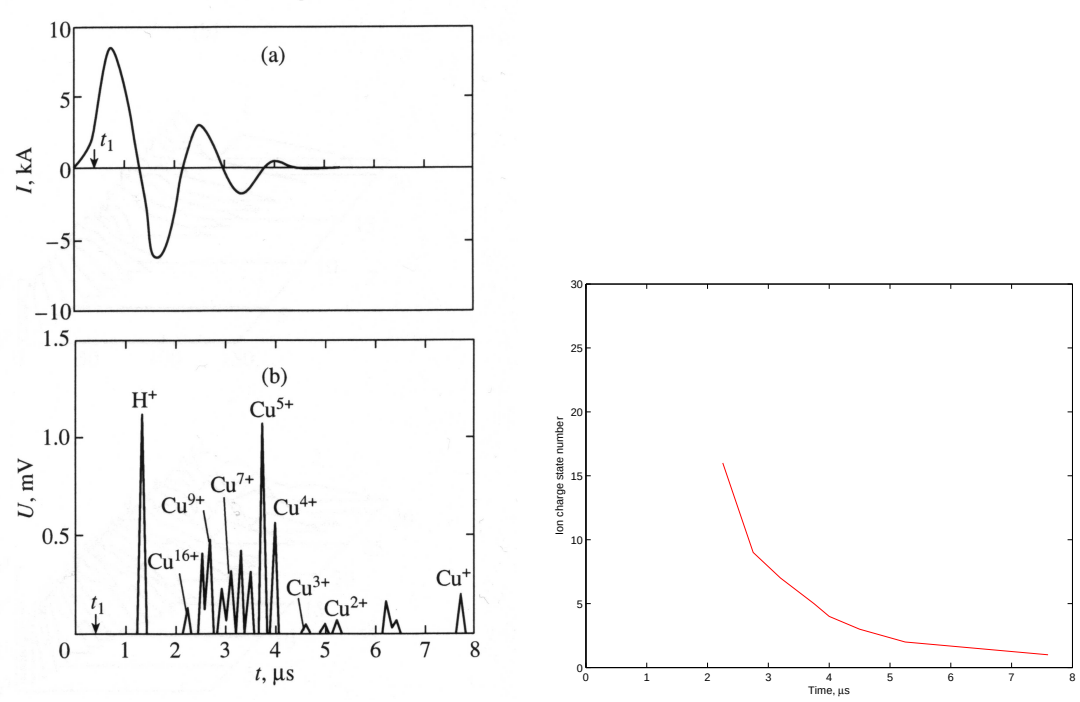

Figure 22. Left: Observed ion states for a 2kV discharge with a 2μF at 40nH capacitor. Right: Decay of the ion charge state over time[36]

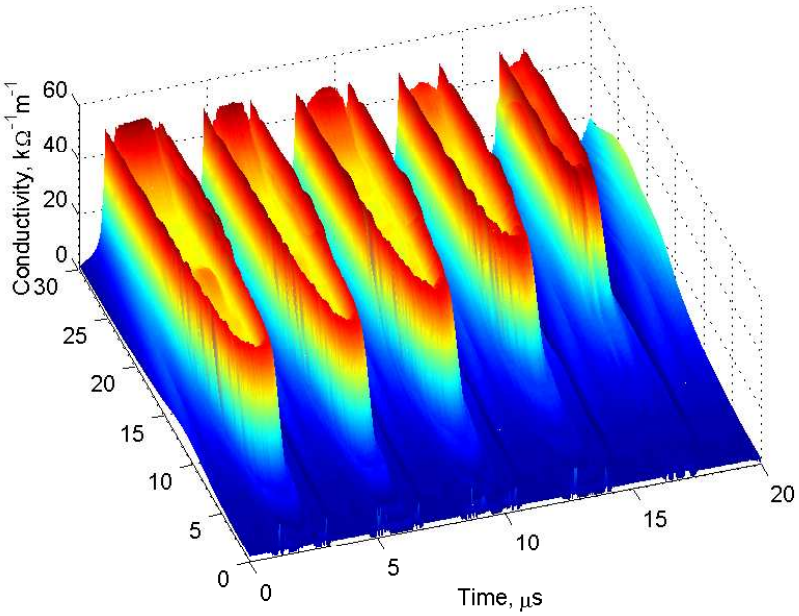

Figure 23. Predicted conductivity for the complete discharge

It should be noted that this is only the mass eroded by the passing current, it does not take into account mass evaporating from cooling emission sites which would increase the total mass loss per pulse without providing significant and useful thrust. Neglecting this mass will have an effect on the calculated total efficiency of the system. It is more appropriate to specify that the efficiency that is being optimised, is the

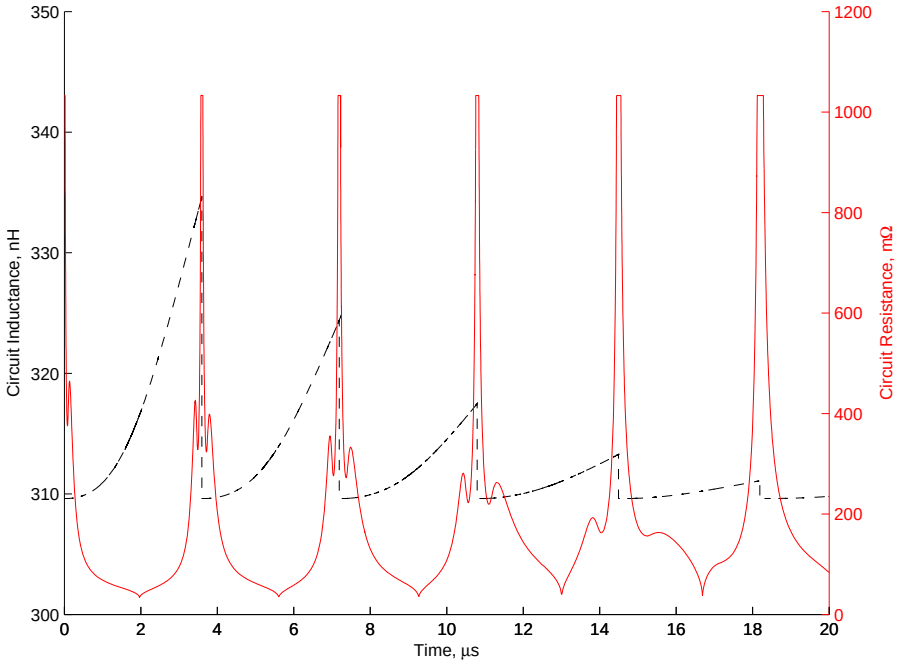

Figure 24. Total plasma resistance of the plasma flow for the complete discharge

efficiency of the system to convert electrical energy into thrust to accelerate the plasma bulk by the Lorentz force:

$$\eta = \frac{E_{kinetic}}{E_0} = \frac{\frac{1}{2}mu_e}{\frac{1}{2}CV_0^2} = \frac{I_{bit}}{CV_0^2} \tag{53}$$

A standard approach is taken to the optimisation process. The PPT model is set up as laid out, arbitrarily, in Table 6. This will be known as the 'standard configuration'. From here one of the parameters under consideration is altered between a range of values whilst all the others are kept the same.

Table 6. Setup of the PPT in the standard configuration

PPT Parameter	Value
High Voltage Capacitor	
Capacitance	4.06μF
Charging voltage	1700V
Cap. Inductance	310nH
Cap. Resistance	33mΩ
Electrodes	
Setup	Parallel bar
Material	Copper
Width	20mm
Thickness	10mm
Separation	30mm

Due to the pulsed nature of the thruster the specific impulse and electrical to kinetic energy conversion efficiency, scales with the plasma bulk speed that varies with time. Figure 25 shows the specific impulse of the PPT in the standard configuration. It also shows the mean and peak specific impulses. The optimisation of the specific impulse and the energy conversion efficiency will consider both the mean and peak values.

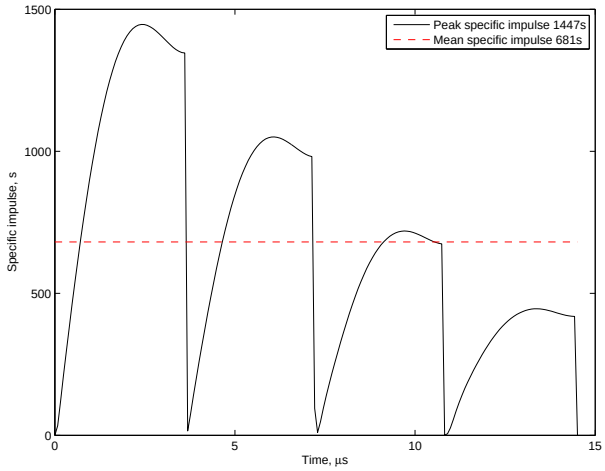

Figure 25. Predicted specific impulse for a PPT setup in the standard configuration. The red dashed line is the mean specific impulse over the whole discharge

The first parameter considered is the charging voltage of the discharge capacitor and is varied between 500V to 2500V, see Figure 26. The upper limit was set to 2500V as above this value for the standard configuration the peak currents produced were of the order of 10kA. Above this peak current the flow model fails to predict the dynamics of the 'choke' region satisfactorily and the model accuracy diminishes. Despite this, the lumped circuit analysis model shows that, as the voltage is increased, all the performance parameters also increase. This is because, as the voltage is increased, the energy of the pulse increases as well. Despite the increase in energy the mean efficiency of the system remains fairly constant but with a gentle rise. Similar distributions are seen when the capacitance of the PPT discharge capacitor is varied over the range of 0.5-8.0μF, see Figure 27. These trends tell us that the efficiency of the system in its ability to use the inputted energy is mostly independent from the energy supplied to the system.

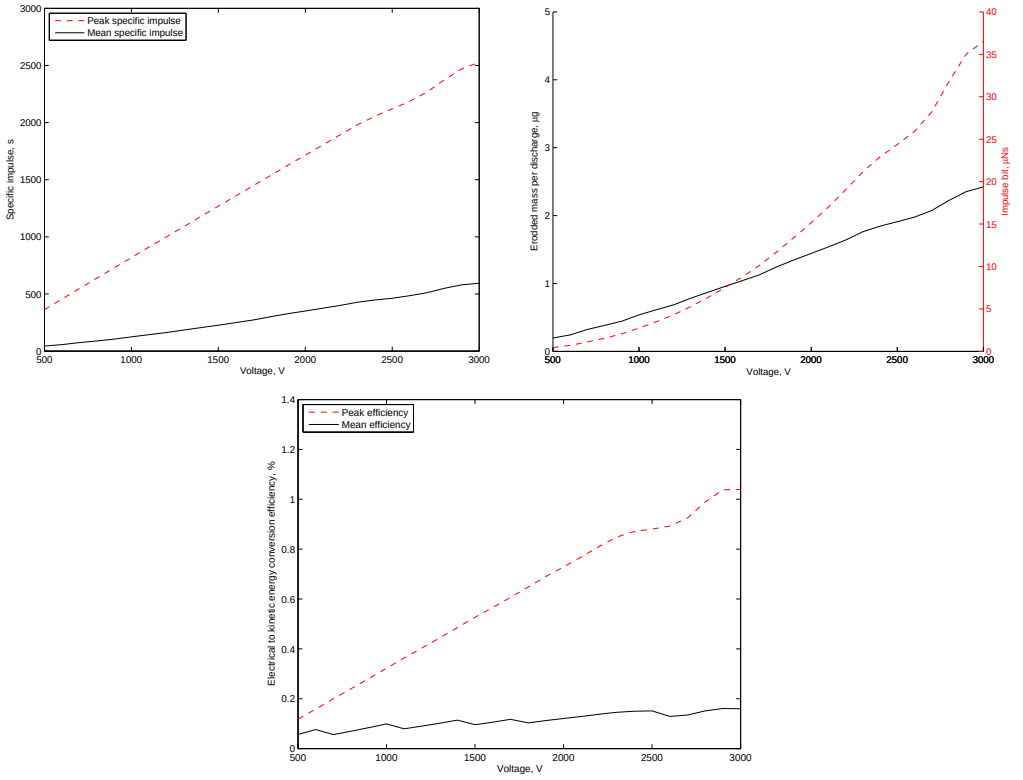

Figure 26. Predicted performance of a PPT setup in the standard configuration but with the discharge voltage being varied from 500-2500V. Top Left: Specific Impulse, Top Right: Impulse bit and mass bit, Bottom: Electrical to kinetic energy conversion efficiency

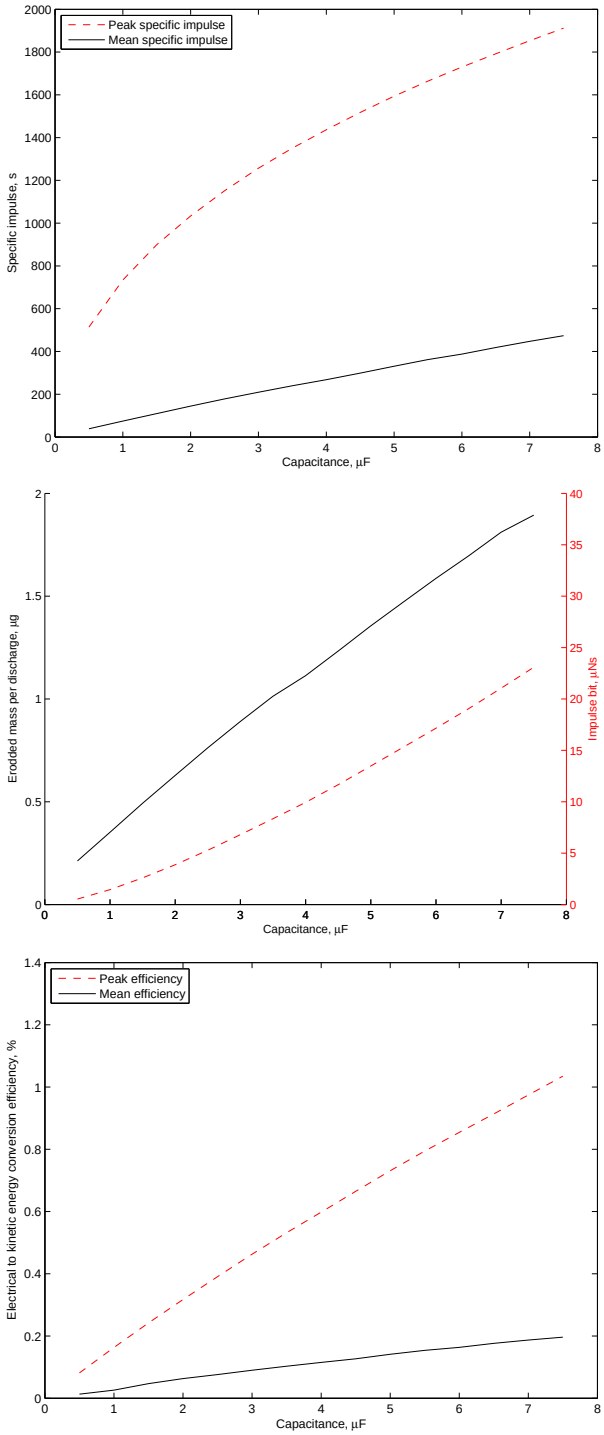

Figure 27. Predicted performance of a PPT setup in the standard configuration but with the PPT capacitor capacitance being varied from 0.5-8.0μF. Top: Specific Impulse, Middle: Impulse bit and mass bit, Bottom: Electrical to kinetic energy conversion efficiency

The inductance of the circuit, which has a significant contribution from the capacitor, was varied between 20-400nH. It is shown that for the standard configuration there is a peak in the impulse bit at approximately 100nH. In general, for the other parameters, as the inductance is increased the performance of the PPT decreases. In the case of the mean specific impulse it remains relatively constant. To improve the PPT performance these trends show that there is a need for the inductance to be matched to the discharge circuit.

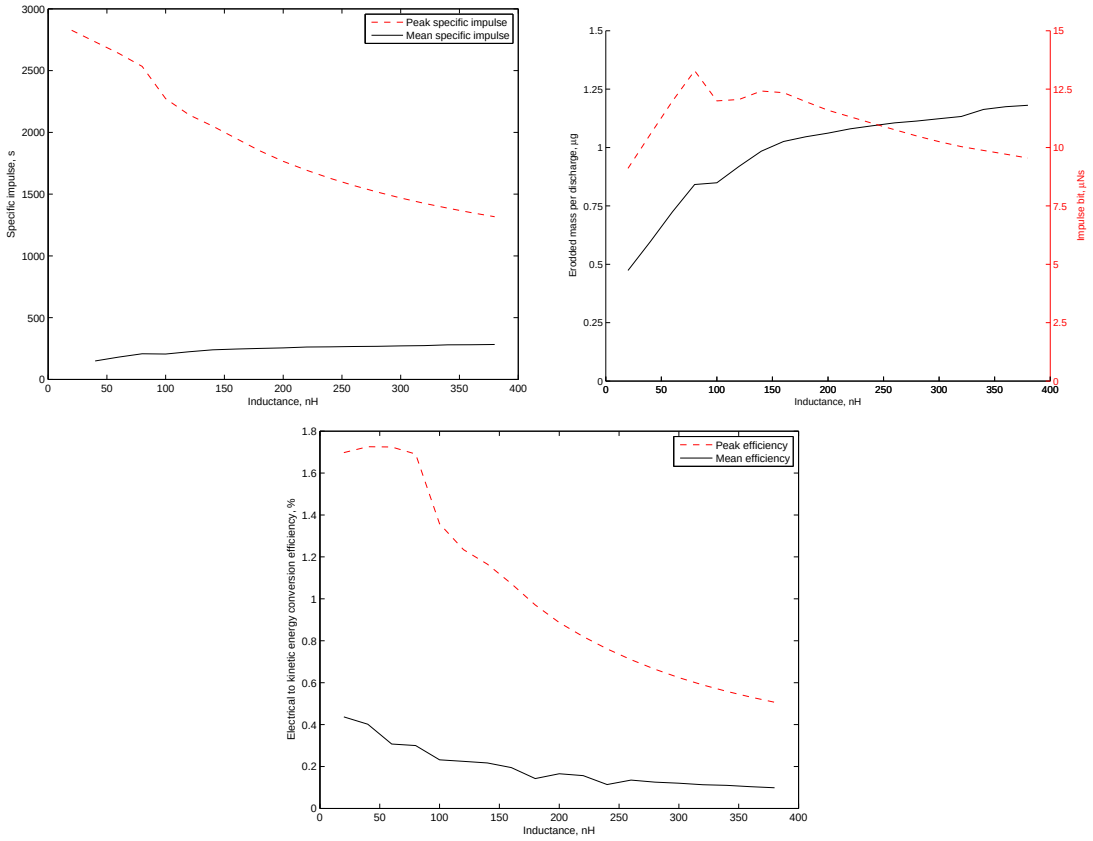

Figure 28. Predicted performance of a PPT setup in the standard configuration but with the circuit inductance being varied from 20-400nH. Top Left: Specific Impulse, Top Right: Impulse bit and mass bit, Bottom: Electrical to kinetic energy conversion efficiency

The total circuit resistance, not including the plasma resistance, was altered from 2-60mΩ. It was observed in Figure 24 that the plasma resistance for the standard configuration can rise up to and above 400 mΩ. Therefore the effect of altering the circuit resistance will be diminished. Figure 29 shows that when the circuit resistance is lowered the impulse bit and specific impulse of the PPT improves. However, the mean efficiency remains relatively constant.

The trends in the circuit resistance and the circuit inductance show that reducing these values in general will lead to performance increases, but care should be taken when lowering the inductance so as not to affect the circuit's ability to store energy in the magnetic field as the pulse rings. Reducing the inductance too much will have a negative effect on the current pulse and the total mass eroded and hence will impact on the impulse bit of the thruster. PPTs should then be developed with low total circuit resistances but properly matched inductances.

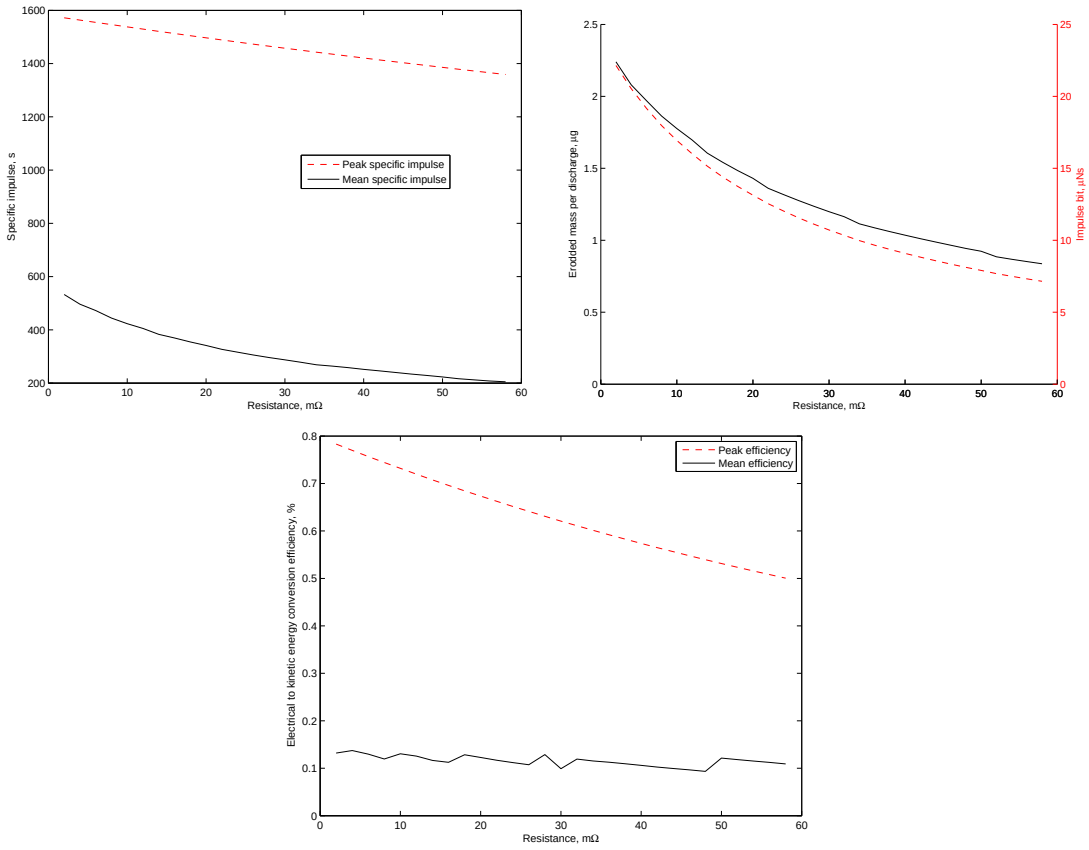

Figure 29. Predicted performance of a PPT setup in the standard configuration but with the circuit resistance being varied from 2-60mΩ. Top Left: Specific Impulse, Top Right: Impulse bit and mass bit, Bottom: Electrical to kinetic energy conversion efficiency

The geometry of the PPT was altered by investigating the electrode gap distance and the electrode thickness. In reality the changes in the geometry to the electrode thickness will not be the same as predicted in this model. In this model the electrode thickness is one of the variables used to map out a rudimentary magnetic field distribution that is used in the Lorentz force model. In that model the midpoint of the electrode thickness represents the distance between the origin point from which the magnetic field distribution emanates (based on two infinitely long wires) and the edge of the electrode, see Equation 47. In the electrode model, see Figure 4, it is shown that the current is not at the centre of the electrodes but towards the corners due to the skin effect. However, despite this inherent inaccuracy of the magnetic field distribution, the variation in the electrode thickness in the force model should provide insight into how to optimise the magnetic field, see Figure 30. The thickness was altered from 1-19mm. In effect the plots show that the closer the origin point of the magnetic field is brought to the electrode surface (i.e. the electrode thickness is reduced) the stronger the magnetic field becomes. This in turn increases the performance of the PPT without affecting the current profile and the mass bit. This trend shows that the performance of the PPT can be enhanced by optimising the magnetic field distribution or by applying an external magnetic field.

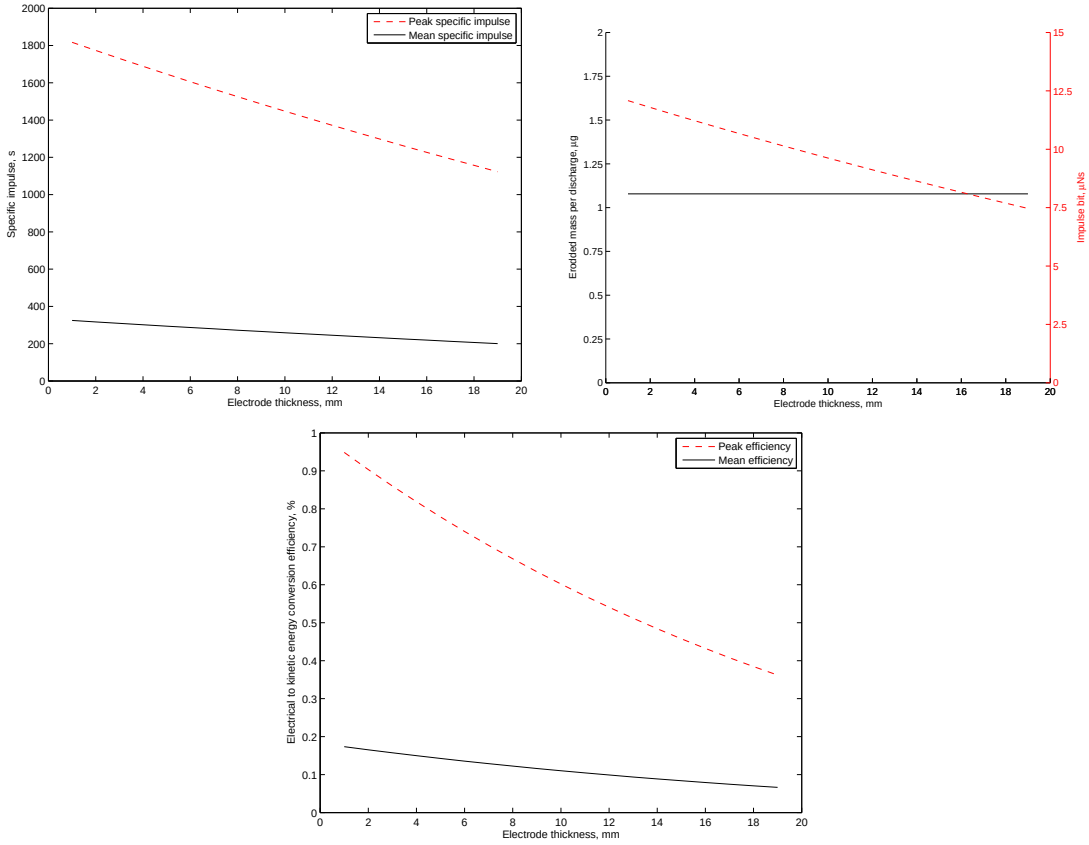

Figure 30. Predicted performance of a PPT setup in the standard configuration but with the electrode thickness being varied from 1-19mm. Top Left: Specific Impulse, Top Right: Impulse bit and mass bit, Bottom: Electrical to kinetic energy conversion efficiency

Finally the electrode gap distance was varied from 5mm to 50mm, see Figure 31. The upper limit of 50mm was chosen because this was the limit of the quasi steady state assumption. As the gap distance is increased to 50mm caution and confidence in the predicted values should be taken. It can be seen that at 18mm, 33mm and 43mm the performance of the PPT dips. Unsurprisingly these coincide with the location of the first and subsequent chokes seen in the plasma flow. In these areas the modelled choke point coincides with the anode and alters the charge-space limited current, predicted by the Child-Langmuir law. However, apart from these dips, the trends show that as the electrode gap is increased the performance rises to a maximum value and remains constant. The location of the choke point as discussed earlier is reliant on the initial flow area and possible anode spot formation processes that are not modelled. The trend shows that for the standard configuration setup the further the electrodes are separated the better the performance will be up to a maximum value. The trends also show that when designing a μPPT the electrodes should be separated as far as possible to maximise the performance.

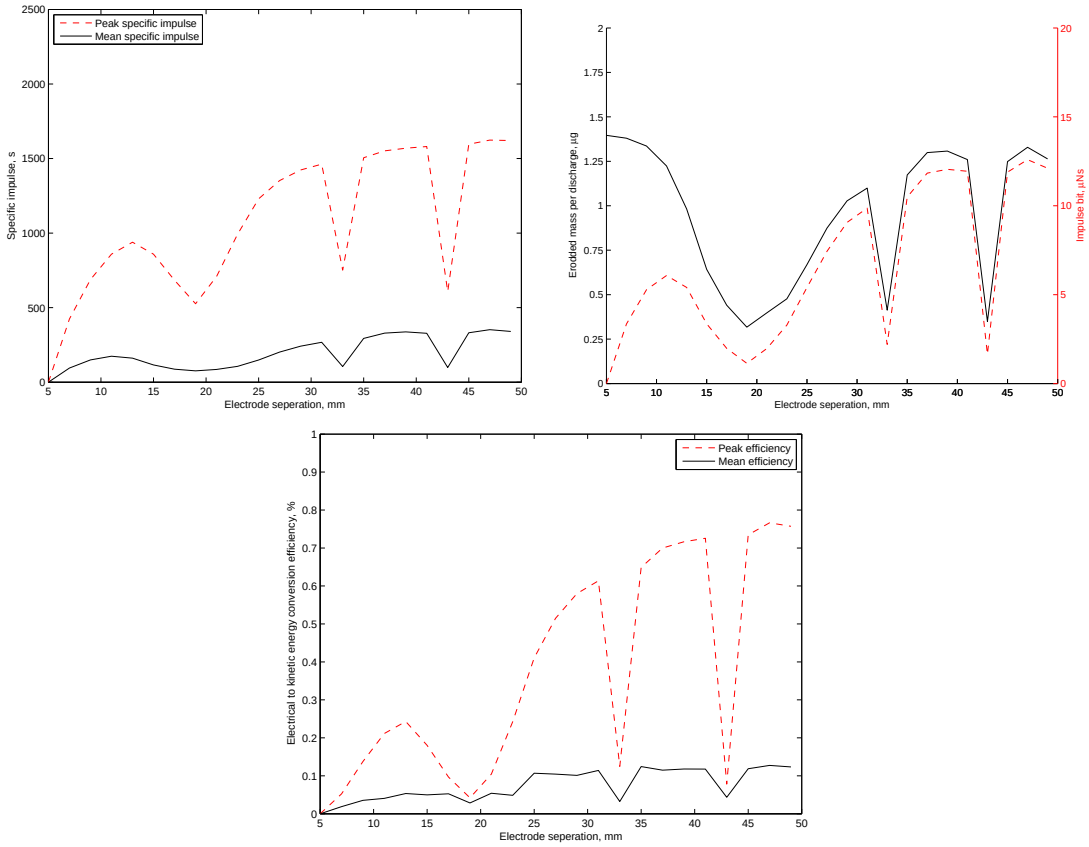

Figure 31. Predicted performance of a PPT setup in the standard configuration but with the electrode separation distance being varied from 5-30mm. Top Left: Specific Impulse, Top Right: Impulse bit and mass bit, Bottom: Electrical to kinetic energy conversion efficiency

It is clear that the PPT discharge is an inefficient process that only converts on average a very small percentage, dependant on the setup, of the total inputted energy into kinetic energy which accelerates the plasma bulk out of the nozzle. Although the peak efficiencies of the individual pulses have been shown to reach higher efficiencies, on the whole the process is still inefficient. It would seem that most of the energy is lost in the charge-space limitation effect brought about by the anode sheath. To improve the performance of the PPT requires the manipulation of the anode sheath in such a way as to limit this effect. Until that can be done the energy conversion efficiency of the PPT from electrical to kinetic energy will remain low.

In summary caution should be taken when evaluating the specific values of the predicted data due to the inaccuracies that may be inherent in the magnetic field distribution of the Lorentz force model and the initial flow radius of the flow model. Despite these, trends can be seen in the produced data that suggest the following should be carried out to optimise the performance of the PPT:

- The circuit resistance, especially that of the capacitor, should be lowered as much as possible.
- The inductance of the circuit should be specifically matched to the PPT to optimise the capability of the circuit to store energy in its magnetic fields as the capacitor discharges.
- The magnetic field distribution should be maximised by optimising the geometry of the PPT or by enhancing the discharge chamber with an external magnetic field.
- The electrode separation distance for copper electrodes should be increased to around 3-5cm but caution should be applied on this upper value as the quasi steady state limit is reached.

VI. Summary

The developed model was based on a lumped circuit analysis model with several additional sub models to predict the behaviour or certain aspects of the thruster. These sub models included a detailed analysis of the discharge electrodes based on splitting the conductor into a number of sub conductors. The resistance, self inductance and mutual inductance was then calculated. It was found that compared to the relative resistance and inductance of the capacitor the electrode resistance and inductance was minimal.

One of the limiting factors of currently avaliable lumped circuit analysis models is the assumption of constant values to describe the plasma that do not fluctuate with time or current. To overcome this lack in modelling a simplified magnetohydrodynamic flow model based on quasi steady state assumptions was put forward. The flow model was based on the assumptions that the plasma mass originated from the electrode surface and flowed towards the anode rather than a plasma bulk originating from a solid propellant between the electrodes (i.e. Teflon^{TM}). The flow model shows that along the flow the plasma at certain distances creates a 'choke', where the flow radius is small. In the 'choke' the electron temperature, electron density and mean ion charge state, significantly rise to values that have been observed in the available literature. The dynamics of the flow has a significant impact on the anode sheath and its ability to limit the arc current. It has been shown that it is this limiting effect that affects the PPT's ability to convert electrical energy to kinetic energy efficiently. If it is possible to manipulate the charge-space of the anode sheath then this is where most gains in performance can be made.

The model has been shown to be a reasonable representation of the effects that occur within a PPT, which does not have Teflon^{TM} present between the electrodes. Future work on improving the model should be focussed on:

- Developing an accurate SPICE model for the discharge capacitor.
- The introduction of anode spots to the flow model.
- Improvement and validation of the Lorentz force model. This will include a more accurate description of the magnetic field distribution from a current carrying rectangular bar in the high frequency domain to account for skin effects and ion speed measurements from time of flight probes.
- Introducing the effects that canting has on the plasma flow.
- Accounting for the initial arc breakdown.
- Optimisation work on the individual cathode spot radii for copper and other materials.

- Reworking the flow model to be time dependant and removing the necessity for steady state assumptions to increase the usability of this model.

References

[1]Shaw, P. and Lappas, V., "Modeling of a Pulsed Plasma Thruster; Simple Design, Complex Matter," 3/6/2010 2010.

[2]Shaw, P. V., Lappas, V. J., and Underwood, C. I., "Design, development and evaluation of an 8 uPPT propulsion module for a 3U CubeSat application," September 1115 2011.

[3]Keidar, M., Boyd, I. D., and Beilis, I. I., "On the model of Teflon ablation in an ablation-controlled discharge," *Journal of Physics D: Applied Physics*, Vol. 34, 2001, pp. 1675–1677.

[4]Keidar, M. and Boyd, I. D., "Optimisation issues for a mico-pulsed plasma thruster," *AIAA*, 2004.

[5]Awadallah, R. S., Freund, D. E., and Simon, D., "Electromagnetic emission modelling for micro pulsed plasma thrusters," *41st Joint propulsion conference*, AIAA, Tucson, Arizona, 2005.

[6]Surzhikov, S. T. and Gatsonis, N. A., "A splitting method of unsteady 3-D magnetogasdynamic flows applied to pulsed plasma thruster plumes," *32nd Plasmadynamics and lasers conference*, AIAA, Anaheim, California, 2001.

[7]Lange, C., *Carbonisation studies on pulsed plasma thruster Teflon propellant*, Ph.D. thesis, Universitat Stuttgart, 2008.

[8]Rhodes, R., Keefer, D., and Thomas, H., "A numerical study of a pulsed plasma thruster," *37th Joint propulsion conference*, AIAA, Salt Lake City, Utah, 2001.

[9]Rooney, D., Moeller, T., Keefer, D., Rhodes, R., and Merkle, C., "Experimental and computer studies of a pulsed plasma accelerator," *43rd Joint propulsion conference*, AIAA, Cincinnati, Ohio, 2007.

[10]Laperriere, D. D., Gatsonis, N. A., and Demetriou, M. A., "Electromechanical modelling of applied field micro pulsed plasma thrusters," *41st Joint propulsion conference*, AIAA, Tucson, Arizona, 2005.

[11]Ziemer, J. K. and Choueiri, E. Y., "Scaling laws for electromagnetic pulsed plasma thrusters," *Plasma Sources Sci. Technol.*, Vol. 10, 2001, pp. 395–405.

[12]Bar, A. W., "Calculation of frequency-dependent impedance for conductors of rectangular cross section," *AMP Journal of Technology*, Vol. 1, 1991, pp. 9.

[13]Nawaz, A., Bauder, U., Bohrk, H. K., Herdrich, G., and Auweter-Kurtz, M., "Electrostatic probe and camera measurements for modeling the iMPD SIMP-LEX," *Jet propulsion conference*, AIAA, 2007.

[14]Anders, A., *Cathodic arcs: From fractal spots to energetic condensation*, Atomic, optical and plasma physics 50, Springer, 1st ed., 2008.

[15]Anders, A., Anders, S., Forsters, A., and Brown, I. G., "Pressure ionisation: its role in metal vapour vacuum arc plasma and ion sources," *Plasma Sources Sci. Technol.*, Vol. 1, 1992, pp. 263–270.

[16]Krinberg, I. A. and Paperny, V., "Cathode jet pinching as the effective mechanism of plasma heating and acceleration," *IEEE 19th International symposium on discharges and electrical insulation in vacuum*, 2000.

[17]Krinberg, I. A. and Paperny, V., "Pinch effect in vacuum arc plasma sources under moderate discharge currents," *Journal of Physics D: Applied Physics*, Vol. 35, 2002, pp. 549–562.

[18]Krasov, V. I., Krinberg, I. A., Paperny, V., Korobkin, Y. V., Romanov, I. V., Rupasov, A. A., and Shikanov, A. S., "Ion acceleration in a high-current cathode plasma jet expanding in vacuum," *Technical Physics Letters*, Vol. 33, No. 11, 2007, pp. 941–944.

[19]Fridman, A. and Kennedy, L. A., *Plasma physics and engineering*, Taylor and Francis, New York, 2004.

[20]Parker, K., "Pulsed plasma thruster plume analysis," *Acta astronautica*, Vol. 53, 2003, pp. 789–795.

[21]Kasperczuk, A., Pisarczyk, T., Kalal, M., Ullschmied, J., Krousky, E., Masek, K., Pfeifer, M., Rohlena, K., Skala, J., Velarde, P., Gonzalez, M., Garcia, C., Oliva, E., and Pisarczyk, P., "Direct and indirect methods of the plasma jet generation," 9 - 13 June 2008.

[22]Nicolai, P., Tikhonchuk, V. T., Kasperczuk, A., Pisarczyk, T., Borodziuk, S., Rohlena, K., and Ullschmied, J., "Plasma jetsproduced in single laser beam interaction with a planar target," 19 - 23 June 2006.

[23]Beilis, I. I., Djakov, B. E., Juttner, B., and Pursch, H., "Structure and dynamics of high-current arc cathode spots in vacuum," *Journal of physics D: Applied physics*, Vol. 30, 1997, pp. 119–130.

[24]Oks, E., Yushkov, G. Y., and Anders, A., "Temporal development of ion beam mean charge state in pulsed vacuum acr ion sources," .

[25]Krinberg, I. A. and Zverev, E. A., "Additional ioization of ions in the inter-electrode gap of a vacuum arc," *Plasma sources sci. Technol.*, Vol. 12, 2003, pp. 7.

[26]Krinberg, I. A., "Three modes of vacuum arc plasma expansion in the absence and presence of a magnetic field," *IEEE Transactions on plasma science*, Vol. 33, No. 5, 2005, pp. 5.

[27]Krinberg, I. A. and Matafonov, G. K., "Control of ion charge states in vacuum arc ion source by imposition of a non-uniform magnetic field," *Surface and Coatings Technology*, Vol. 201, 2007, pp. 4.

[28]Krinberg, I. A., "Plasma flow crisis and the limiting electron temperature in a vacuum arc in axial magnetic field," *Technical Physics Letters*, Vol. 31, No. 3, 2004, pp. 3.

[29]D., H. J., "NRL Plasma Formulary," Tech. rep., Beam Physics Branch, Plasma Physics Division, Naval Research Laboratory, 2007 2007.

[30]Zverev, E. A. and Krinberg, I. A., "The current coloumn contraction and ion charge increase induced by the current build up in a pulsed vacuum discharge," *Technical Physics Letters*, Vol. 26, No. 4, 2000, pp. 3.

[31]Korobkin, Y. V., Paperny, V., Romanov, I. V., Rupasov, A. A., and Shikanov, A. S., "Micropinches in laser induced moderate power vacuum discharge," *Plasma Phys. Control. Fusion*, Vol. 50, 2008, pp. 14.

[32]Anders, A., Oks, E., Yushkov, G. Y., Savkin, K. P., Brown, I. G., and Nikolaev, A., "Measurements of the total ion flux from vacuum arc cathode spots," *IEEE Transactions on plasma science*, Vol. 33, No. 5, 2005, pp. 4.

[33]Kumagai, N., Igarashi, M., Sato, K., Tamura, K., Kawahara, K., and Takegahara, H., "Plume diagnostics in pulsed plasma thruster," *38th Joint propulsion conference*, AIAA, Indianapolis, Indiana, 2002.

[34]Zwahlen, J. C., *Investigation of a pulsed plasma thruster plume using a quadruple langmuir probe technique*, Ph.D. thesis, Worcester Polytechnic Institute, 2002.

[35]Gatsonis, N. A., Zwahlen, J. C., Wheelock, A., Pencil, E. J., and Kamhawi, H., "Characterization of a pulsed plasma thruster plume using a quadruple langmuir probe method," *38th Joint propulsion conference*, AIAA, Indianapolis, Indiana, 2002.

[36]Artamonov, M. F., Krasov, V. I., and Paperny, V., "Registration of accelerated multiply charged ions from the cathode jet of a vacuum discharge," *Journal of Experimental and Theoretical Physics*, Vol. 93, No. 6, 2001, pp. 5.